



# Dominance of large-scale atmospheric circulations in long-term variations of winter PM<sub>10</sub> concentrations over East Asia

Greem Lee<sup>a</sup>, Chang-Hoi Ho<sup>a,\*</sup>, Lim-Seok Chang<sup>b</sup>, Jinwon Kim<sup>c</sup>, Maeng-Ki Kim<sup>d</sup>, Seong-Joong Kim<sup>e</sup>

<sup>a</sup> School of Earth and Environmental Sciences, Seoul National University, 1, Gwanak-ro, Gwanak-gu, Seoul, Republic of Korea

<sup>b</sup> Air Quality Forecasting Center, National Institute of Environmental Research, 42, Hwangyeong-ro, Seogu, Incheon, Republic of Korea

<sup>c</sup> Climate Research Division, National Institute of Meteorological Sciences, 33, Seohobuk-ro, Seogwipo-si, Jeju-do, Republic of Korea

<sup>d</sup> Department of Atmospheric Science, Kongju National University, 56, Gongjudaehak-ro, Gongju-si, Chungcheongnam-do, Republic of Korea

<sup>e</sup> Division of Polar Climate Sciences, Korea Polar Research Institute, 26, Songdomirae-ro, Yeosu-si, Incheon, Republic of Korea

## ARTICLE INFO

### Keywords:

Particulate matter  
PM<sub>10</sub>  
Atmospheric circulation  
Ural blocking  
East Asia

## ABSTRACT

Concentrations of wintertime particulate matters of diameters below 10 μm (PM<sub>10</sub>) in South Korea and China have decreased since the 2000s largely owing to the emissions reduction policies of the two countries; however, this decreasing tendency has been notably weakened, or even been reversed, in recent years. This study examines the influence of large-scale atmospheric circulations on this PM<sub>10</sub> change over East Asia for the winters (December–February) of the 2004/05–2015/16 period using an empirical orthogonal function (EOF) analysis. The first EOF mode, which accounts for 32.7% of the total variance, indicates decreases in PM<sub>10</sub> concentrations until 2012 and thereafter increases in them particularly at most stations in eastern and northeastern China. Regression patterns of meteorological variables with respect to the first EOF time series indicate that the wintertime PM<sub>10</sub> variations over East Asia are greatly influenced by the Ural blocking; the weakening of the Ural blocking after 2014 led to the weakening of cold air flows from the north and provided atmospheric conditions favorable for bad air quality events over East Asia. The second EOF mode, which accounts for 20.1% of the total variance, shows a similar spatial distribution as the linear trend of PM<sub>10</sub> concentrations during the analysis period and would be related to the long-term changes in emissions. Our findings emphasize that the long-term variations in air quality over East Asia are affected primarily by the variations in large-scale atmospheric circulations with secondary contributions from the changes in emissions.

## 1. Introduction

Particulate matters of diameters below 10 μm (PM<sub>10</sub>) exert seriously adverse effects on human health (Dockery and Pope, 1994; Harrison and Yin, 2000; Hong et al., 2002) as well as visibility, which is a major cause of traffic problems, agriculture, and ecosystems (Chen et al., 2013b; Grantz et al., 2003; Hyslop, 2009). Exposure to PM<sub>10</sub> leads to increases in respiratory and cardiovascular diseases which are responsible for about a million premature deaths worldwide annually (Cohen et al., 2005). The World Health Organization (WHO) has set thresholds for the annual and 24-h average levels of PM<sub>10</sub> at 20 and 50 μg m<sup>-3</sup>, respectively, as a guide for reducing the adverse health effects (WHO, 2006). In accordance with the WHO recommendations, many developed and developing countries have been controlling air quality using their own standards. The current air quality standards for PM<sub>10</sub> in South Korea and urban areas in China, for instance, are 50 and 70 μg m<sup>-3</sup>, respectively, for the annual mean and are 100 and

150 μg m<sup>-3</sup>, respectively, for the 24-h mean (China's Ministry of Environmental Protection, 2012; Korea Ministry of Environment, 2017).

In South Korea, nationwide measures to improve air quality have been implemented since the early 2000s under the “National Environmental Comprehensive Plans” which includes upgrade in the quality of fossil fuels, regulation of the amount of air pollutants emitted from factories, and the replacement of diesel buses with natural gas buses (Kim and Shon, 2011a,b). These 10-year policies and specific measures established every year (Korea Ministry of Environment, 2015) have steadily decreased the air pollutant emissions and PM<sub>10</sub> concentrations until 2012 (Kim et al., 2015; Kim et al., 2019; Oh et al., 2015, 2018); however, since 2013, the trend of decreasing PM<sub>10</sub> concentrations is stopped noticeably (Kim et al., 2017b; Lee et al., 2018b). In China, “Joint Prevention and Control of Air Pollution” and “Action Plan on Prevention and Control of Air Pollution” were issued to prevent and control air pollution and to meet the National Ambient Air Quality

\* Corresponding author at: 501-406, Seoul National University, 1, Gwanak-ro, Gwanak-gu, Seoul, Republic of Korea.

E-mail address: [hoch@cpl.snu.ac.kr](mailto:hoch@cpl.snu.ac.kr) (C.-H. Ho).

<https://doi.org/10.1016/j.atmosres.2020.104871>

Received 3 July 2019; Received in revised form 28 December 2019; Accepted 20 January 2020

Available online 21 January 2020

0169-8095/ © 2020 Elsevier B.V. All rights reserved.

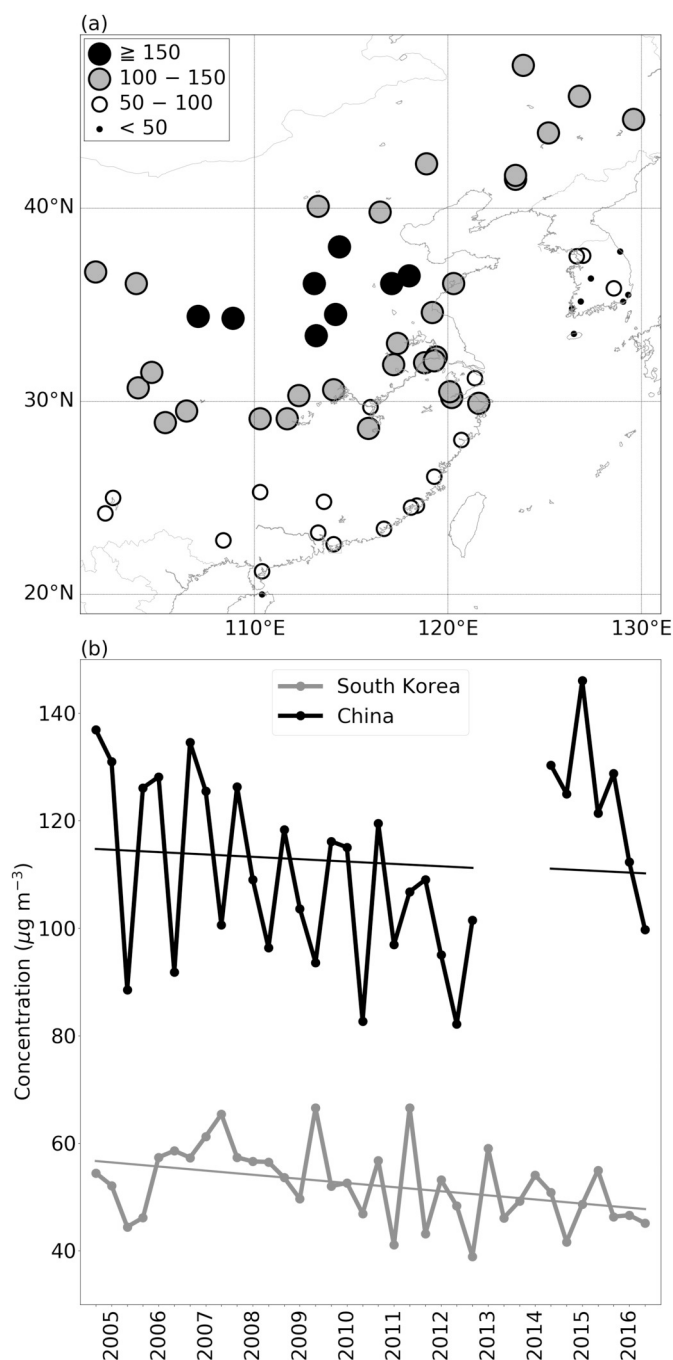


**Fig. 1.**  $\text{PM}_{10}$  concentrations ( $\mu\text{g m}^{-3}$ ) over East Asia in 2004/05–2015/16; (a) Winter-month (December–February) average. (b) Domain average in South Korea (10 regions) and China (54 regions). Years on the x-axis are marked in January. Gray and black straight lines depict least-squares regression: In terms of the gray (black) line, slope =  $-0.26 \mu\text{g m}^{-3} \text{ month}^{-1}$ ,  $p = .02$  (slope =  $-0.15 \mu\text{g m}^{-3} \text{ month}^{-1}$ ,  $p = .66$ ).

Standards (NAAQS) (Zhang et al., 2016). These plans include the implementation of simultaneous controls of multiple pollutants and regional air pollution, developments of clean-energy resources, enhancements of vehicle and industrial pollution control, and the establishment of monitoring and early-warning systems for air pollution and other supportive policies (Fu and Chen, 2017; Zhang et al., 2016; Zheng et al., 2018). The air pollutant emissions and  $\text{PM}_{10}$  concentrations in major regions in China have consistently declined with strict

implementation of these reduction policies (Xu et al., 2016a; Zheng et al., 2018), particularly after the award to host the Beijing Olympic Games (Chen et al., 2018; Xu et al., 2016b; Zhang et al., 2016). However,  $\text{PM}_{10}$  concentrations showed abrupt jumps during 2013–2015 mainly in eastern and northeastern China resulting from frequent occurrence of severe haze episodes in winter (Chang et al., 2016; Hung et al., 2018; Li et al., 2016; Wang et al., 2014; Yan et al., 2015; Zhang et al., 2018b). The worsening of air quality in China has also affected air quality in South Korea (Kim et al., 2016; Kim et al., 2017a; Koo et al., 2018; Seo et al., 2017); For instance, Kim et al. (2017a) simulated that Chinese sources contributed 64% of  $\text{PM}_{10}$  mass concentrations in the Seoul Metropolitan Area during late February 2014.

The principal factors that control regional air quality include emissions of air pollutants (Behera et al., 2015; Fu et al., 2008), large-scale circulation and associated regional meteorology (Han et al., 2014; Jang et al., 2017; Lee et al., 2018a; Yang et al., 2015; You et al., 2017, 2018), and the formation of secondary aerosols (Behera et al., 2015; Han et al., 2014). Several studies reported that large-scale atmospheric circulations play an important role in the degradation of air quality by inducing adverse local meteorological conditions such as surface high-pressure systems and weak winds (Lee et al., 2011; Oh et al., 2015, 2018; Shu et al., 2017; Wai and Tanner, 2005; Zhao et al., 2018). With regard to the recent variations of  $\text{PM}_{10}$  concentrations in East Asia, Chang et al. (2016) suggested that weak southeasterlies over eastern China induced by the December 2015 El Niño event caused severe haze events over the region. Shu et al. (2017) reported that strong westerlies transported air pollutants from the Beijing–Tianjin–Hebei region and Sichuan Basin into the Yangtze River Delta (YRD) in 2013–2014 when the East Asian trough, one of common features of the East Asian winter monsoon (EAWM) (Wang et al., 2009), was located to the east of the YRD. Zhao et al. (2018) demonstrated that, during a cold Arctic period in January 2013, a strong polar vortex and relevant westerlies in the mid-troposphere resulted in a weak Siberian High over Eurasia, which in turn induced weak surface northwesterlies and high air pollutant levels over China. Seo et al. (2017) found that a severe multiday haze episode in South Korea in February 2014 was due to a stagnant weather condition induced by atmospheric blocking over Alaska developed from a planetary wave ridge. Studies on the relationship between the recent changes in  $\text{PM}_{10}$  concentrations over East Asia and the variations in large-scale atmospheric circulations are still ongoing.

This study examines the observed temporal changes in  $\text{PM}_{10}$  concentrations during winters (December–February) of 2004/05–2015/16 in South Korea and China. We employ an empirical orthogonal function (EOF) analysis to understand the effect of large-scale atmospheric circulations on the observed variations in  $\text{PM}_{10}$  concentrations over East Asia. It is found that the weakening of the Ural blocking provides atmospheric conditions favorable for bad air quality events over East Asia by analyzing regression patterns of meteorological variables with respect to the leading EOF mode. To the authors' knowledge, there is no research on the relationship between air quality in East Asia and the intensity of the Ural blocking. The data and method are described in Section 2. The results of the EOF analysis of  $\text{PM}_{10}$  concentrations over East Asia and the regressed atmospheric variables with respect to the first EOF time series are presented in Section 3. The discussion is given in Section 4. The summary is in Section 5.

## 2. Data and method

### 2.1. Data

Hourly  $\text{PM}_{10}$  concentrations in South Korea measured using Thermo FH62C-14 (USA) and Kimoto PM-711 (Japan) were obtained from the

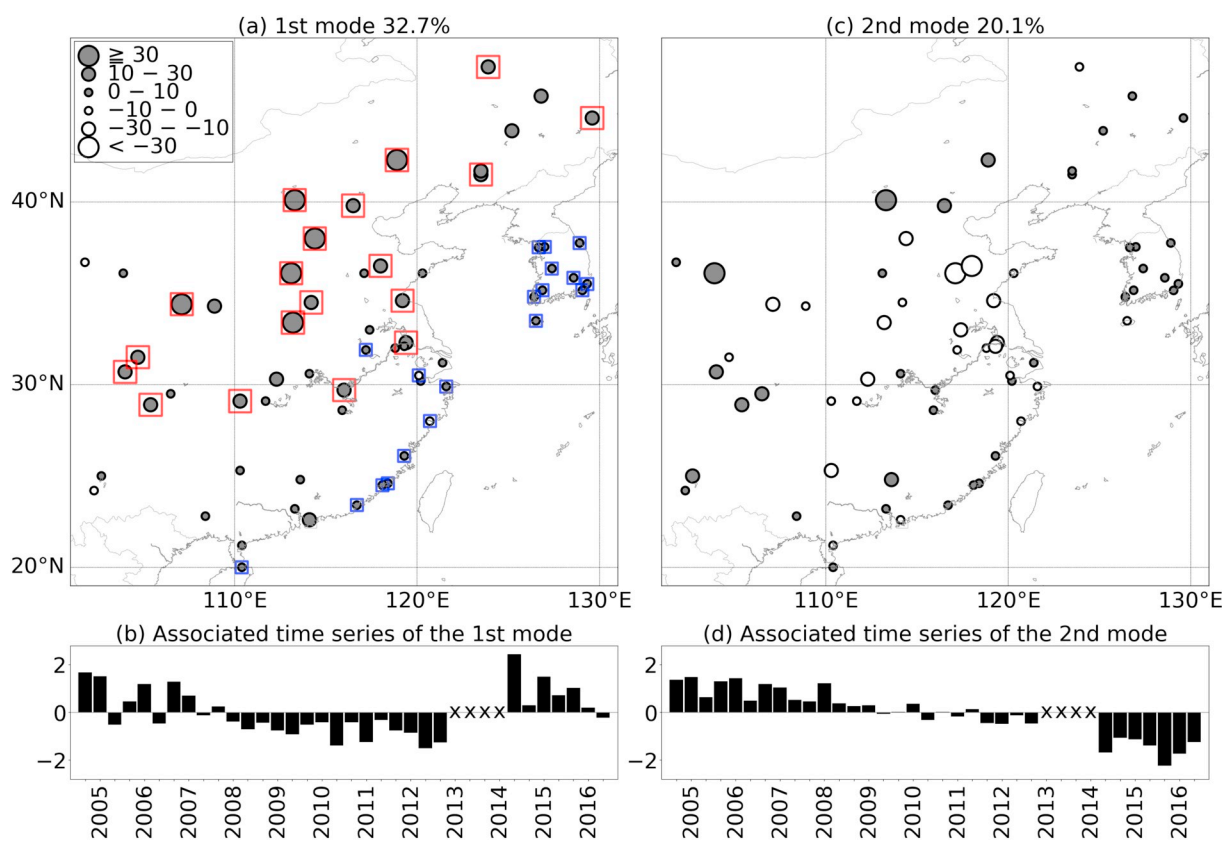


**Fig. 2.** (a) and (b) The first EOF mode of winter  $PM_{10}$  concentrations over East Asia in 2004/05–2015/16; (a) Eigenvector and (b) associated time series. (c) and (d) The same as that in (a) and (b), respectively, for the second EOF mode. Numbers 32.7% and 20.1% in (a) and (c) indicate the variances of the first and second modes, respectively. The red and blue squares in (a) depict R1 and R2 regions, respectively (see Fig. 5 later), with the highest and lowest eigenvectors (upper and lower 30%, i.e., 19 regions each) of the first EOF mode. Years on the x-axis of (b) and (d) are marked in January. (For interpretation of the references to colour in this figure legend, the reader is referred to the web version of this article.)

National Institute of Environmental Research (<http://www.airkorea.or.kr>). The accuracy, precision, and detection range of Thermo are  $\pm 5\%$ ,  $\pm 2 \mu\text{g m}^{-3}$ , and  $1\text{--}10,000 \mu\text{g m}^{-3}$ , respectively; those of Kimoto are  $\pm 1\%$ ,  $\pm 2 \mu\text{g m}^{-3}$ , and  $0.5\text{--}5000 \mu\text{g m}^{-3}$ , respectively.  $PM_{10}$  mass concentrations were measured using the beta-ray absorption method (Kim and Kim, 2003), whose measurement error caused by particle-containing moisture is known to be 10% (Chang and Tsai, 2003). The monthly mean concentrations in 10 cities<sup>1</sup> (see stations in Fig. 1a)—the capital (Seoul with 27 sites), six metropolitan cities (Incheon, Daejeon, Gwangju, Daegu, Ulsan, and Busan with 16, 8, 7, 11, 14, and 19 sites, respectively), and three cities (Gangneung, Mokpo, and Jeju with one, two, and two sites, respectively)—were employed in this study. The Asian dust days (Table S1) were excluded using the Asian dust data from the Korea Meteorological Administration (KMA) (<http://www.weather.go.kr/weather/asiandust/observday.jsp>) in order to isolate the effects of anthropogenic  $PM_{10}$  (Hur et al., 2016; Lee et al., 2018b; Oh et al., 2015, 2018).

In China, the Tapered Element Oscillating Microbalance (TEOM, model 1400a, Rupprecht & Patashnick, USA) and Beta-ray Attenuation Monitor (BAM-1020, Met One, USA) are two kinds of instruments used at monitoring sites to measure  $PM_{10}$  mass concentrations. The accuracy, precision, and detection range of TEOM are  $\pm 0.75\%$ ,  $\pm 1.5 \mu\text{g m}^{-3}$ , and  $0\text{--}5000000 \mu\text{g m}^{-3}$ , respectively (<https://assets.thermofisher.com/TFS-Assets/LSG/Specification-Sheets/D19391~.pdf>); those of BAM-1020 are  $\pm 2\%$ ,  $\pm 4\text{--}5 \mu\text{g m}^{-3}$ , and  $0\text{--}10000 \mu\text{g m}^{-3}$ , respectively (Lee et al., 2006; <http://webbook.me.go.kr/DLI-File/NIER/09/020/5592612.pdf>). Their calibration, validation, and data quality control

are supported by China National Environmental Monitoring Center (China's Ministry of Environmental Protection, 2013; Xu et al., 2017). The uncertainty of the daily  $PM_{10}$  measurement is typically  $< 1\%$  (Xia et al., 2006). China's Ministry of Ecology and Environment (MEE) converts  $PM_{10}$  concentrations into indices, such as the Air Pollution Index (API) and Air Quality Index (AQI), and releases them publicly (<http://datacenter.mee.gov.cn/>). The API and AQI in China were collected for 54 stations<sup>1</sup> (Fig. 1a) selected based on the data availability for 2004/05–2015/16. For December 2004–December 2012,  $PM_{10}$  concentrations were converted from the API using Eq. (1),

$$PM_{10} = \frac{API - API_{low}}{API_{high} - API_{low}} \times (PM_{10\ high} - PM_{10\ low}) + PM_{10\ low} \quad (1)$$

where  $API_{high}$  and  $API_{low}$  are the values that correspond to the upper and lower NAAQS API standard, respectively;  $PM_{10\ high}$  and  $PM_{10\ low}$  are the standard concentration values corresponding to  $API_{high}$  and  $API_{low}$ , respectively (Zhang et al., 2003). We only used API on days when  $PM_{10}$  had been reported as the principal pollutant. Because the AQI has replaced API for the air pollution network since 2013,  $PM_{10}$  mass concentrations in February 2014–February 2016 were converted from AQI using Eq. (2),

$$PM_{10} = \frac{AQI - AQI_{low}}{AQI_{high} - AQI_{low}} \times (PM_{10\ high} - PM_{10\ low}) + PM_{10\ low} \quad (2)$$

where  $AQI_{high}$  and  $AQI_{low}$  are the values that correspond to the upper and lower AQI standard, respectively, of the US Environmental Protection Agency air quality standards, and  $PM_{10\ high}$  and  $PM_{10\ low}$  are the standard concentrations corresponding to  $AQI_{high}$  and  $AQI_{low}$ , respectively (Zheng et al., 2014). For the data availability, we used AQI of

<sup>1</sup> The locations and names of observed stations are displayed in Fig. S1.

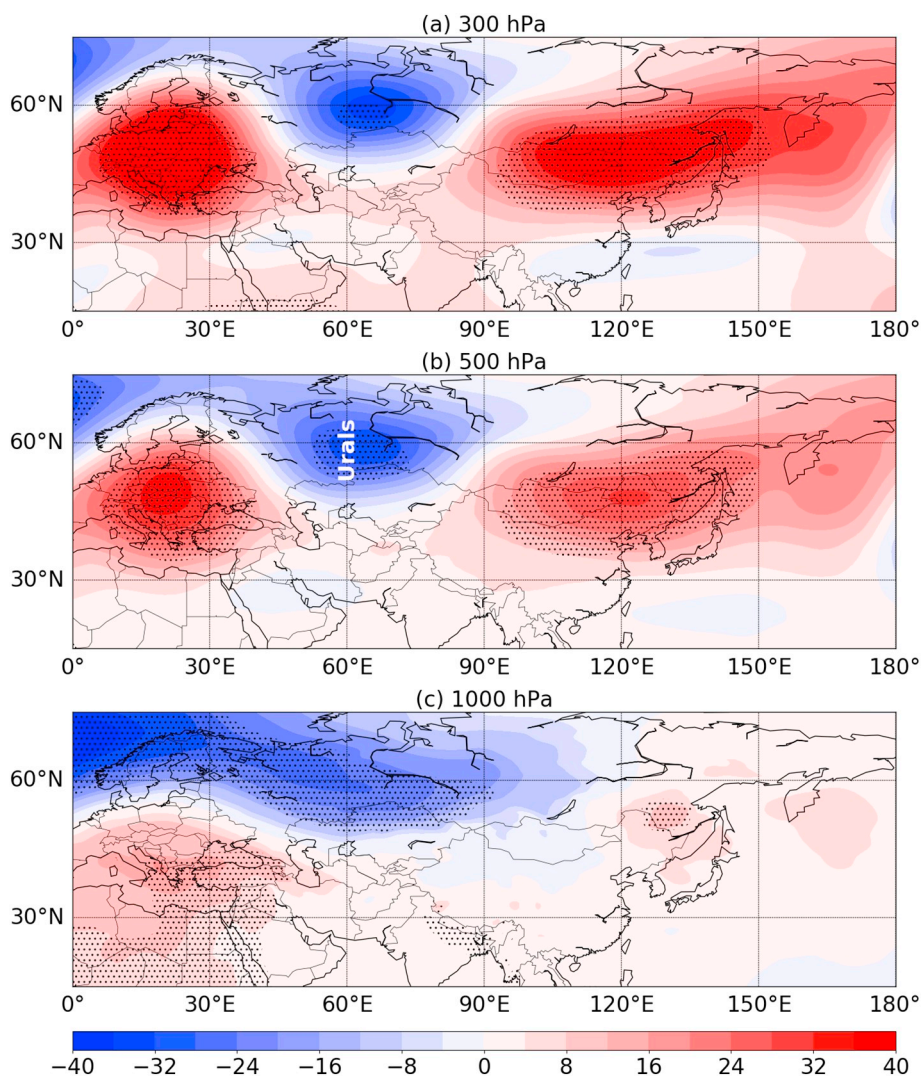


Fig. 3. Regressed geopotential height anomalies (gpm) at (a) 300, (b) 500, and (c) 1000 hPa with respect to the first EOF time series (Fig. 2b). The dots indicate that the value is significant at the 95% confidence level. The coordinates of the Ural Mountains are (60°N, 60°E).

PM<sub>10</sub> collected from the World Air Quality Index Project (<http://aqicn.org>) on which the Chinese government provides the official AQI data (<http://aqicn.org/sources/>). Although API differs from AQI, several studies used both data to evaluate air quality because they are comparable and are well correlated to each other (Hur et al., 2016; Liu et al., 2016; Zhou et al., 2017). From the period 2004/05–2015/16, we excluded the period from January 2013 to January 2014 because the timing of the transition from API to AQI varies for different stations and thus only few stations provide the data in this period. The Asian dust days in China were also excluded using the Asian dust data in synoptic observation reports (the meteorological reports sent worldwide by the World Meteorological Organization through the Global Telecommunication System) obtained from KMA. Several previous studies have used the same API, AQI (Hur et al., 2016; Lee et al., 2013; Oh et al., 2015), and Asian dust data (Lee et al., 2015).

Monthly Aerosol optical thickness (AOT) with a 0.5° × 0.5° latitude-longitude grid from the Moderate Resolution Imaging Spectroradiometer onboard the Terra satellite (MODIS/Terra) obtained from the National Aeronautics and Space Administration (NASA) Earth Observations (<https://neo.sci.gsfc.nasa.gov/>) and PM<sub>2.5</sub> concentrations observed by the United States (US) Department of State Air Quality

Monitoring Program (<http://stateair.net>) were utilized to further evaluate the continuity of API and AQI and to determine whether the two data can be used together.

To investigate large-scale atmospheric circulations, the monthly mean geopotential height and wind at 300, 500, and 1000 hPa and surface air temperature, sea surface temperature, and sea ice cover were obtained from the interim European Centre for Medium-Range Weather Forecasts *Re-Analysis* data with a 0.5° × 0.5° grid (Dee et al., 2011). The snow cover with a 0.05° × 0.05° grid from the MODIS/Terra was obtained from the NASA National Snow and Ice Data Center (Hall and Riggs, 2015). The monthly means and anomalies of these data were used in the analyses. The Arctic Oscillation (AO) index data was downloaded from the Climate Prediction Center of the National Oceanic and Atmospheric Administration (NOAA) ([https://www.cpc.ncep.noaa.gov/products/precip/CWlink/daily\\_ao\\_index/ao.shtml](https://www.cpc.ncep.noaa.gov/products/precip/CWlink/daily_ao_index/ao.shtml)).

## 2.2. Method

An EOF analysis was carried out to examine the spatiotemporal variation of PM<sub>10</sub> concentrations over East Asia. This analysis is useful for decomposing a dataset into a set of mathematically independent

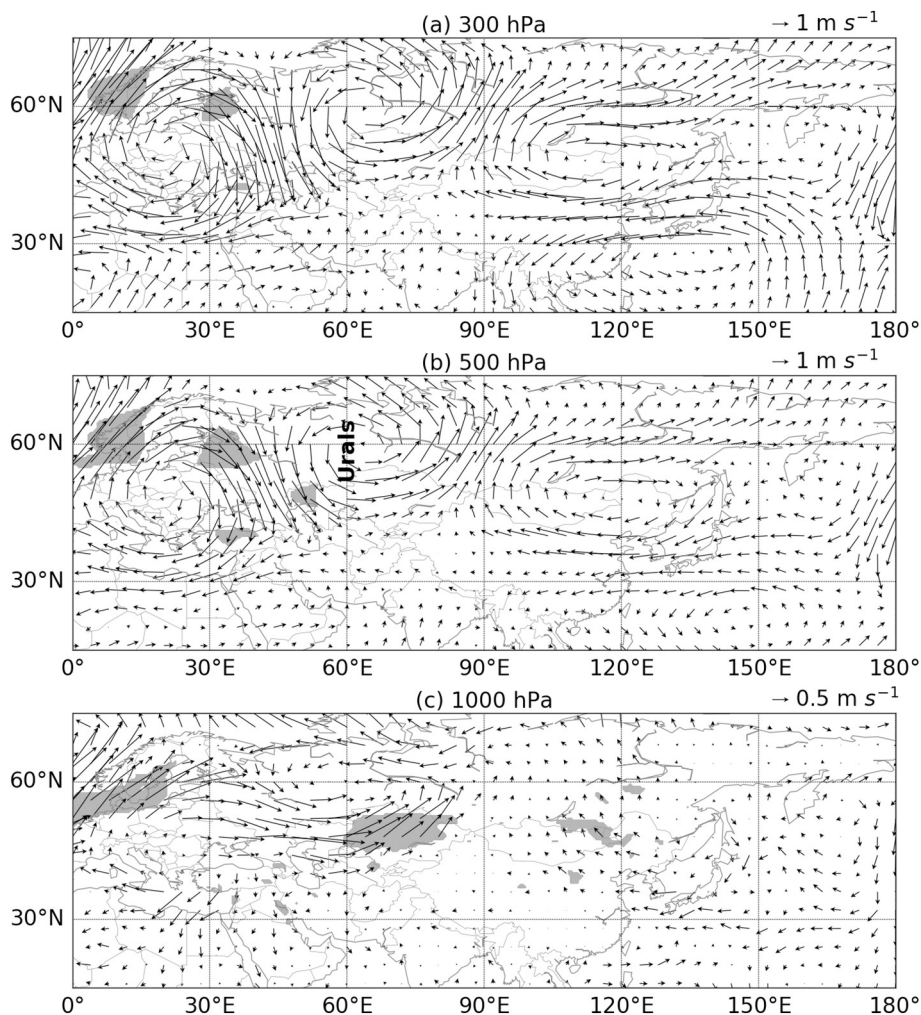


Fig. 4. The same as that shown in Fig. 3 except for wind anomalies ( $\text{m s}^{-1}$ ). The shades indicate that the value is significant at the 95% confidence level. The coordinates of the Ural Mountains are ( $60^\circ\text{N}$ ,  $60^\circ\text{E}$ ).

structures that explain the variance in the dataset as efficiently as possible. Many studies employed this analysis for air quality researches (e.g., Fischer et al., 2011; Sanap and Pandithurai, 2015; Zhai et al., 2015). The EOF analysis extracts orthogonal spatiotemporal variation patterns from the data and a few dominant modes generally account for a large part of the total variance and can be related to physical phenomena. The EOF analysis was conducted by using the *eofs* library for Python (Dawson, 2016).

The Ural blocking frequency was used as a blocking index (Cheung et al., 2012, 2015; Luo et al., 2016; Yao et al., 2017). According to the blocking identification method of Tibaldi and Molteni (1990), the index is defined in terms of the 500-hPa geopotential height  $Z$  difference between three latitudes,  $\varphi_N = 80^\circ\text{N} + \Delta$ ,  $\varphi_0 = 60^\circ\text{N} + \Delta$ , and  $\varphi_S = 40^\circ\text{N} + \Delta$ . The criteria are

$$\text{GHGN} = \frac{Z(\varphi_N) - Z(\varphi_0)}{\varphi_N - \varphi_0} < -10 \text{ gpm } (^\circ\text{lat})^{-1} \quad (3)$$

$$\text{GHGS} = \frac{Z(\varphi_0) - Z(\varphi_S)}{\varphi_0 - \varphi_S} > 0 \quad (4)$$

where GHGN and GHGS denote the 500-hPa  $Z$  gradients in the higher- and lower-latitude regions for each given longitude, respectively. A five-day moving average was applied prior to calculating the index and

$\Delta = -5^\circ, -2.5^\circ, 0^\circ, 2.5^\circ, \text{ or } 5^\circ$  over  $45^\circ\text{E}$ – $90^\circ\text{E}$  were used in this study. A blocking index is referred to have occurred if the above criteria are satisfied by at least one of the five latitude pairs, at least  $12.5^\circ$  consecutive blocking longitudes, and for at least three consecutive days.

The Siberian High intensity was defined as the mean sea level pressure within  $40^\circ\text{N}$ – $65^\circ\text{N}$  and  $80^\circ\text{E}$ – $120^\circ\text{E}$ , where the maximum sea level pressure center is found in winter. The same or similar definitions of the Siberian High intensity have been utilized in many previous researches (Gong and Ho, 2002; Jeong et al., 2011; Wu and Wang, 2002). Similarly, the Aleutian Low intensity was defined as the mean sea level pressure within  $30^\circ\text{N}$ – $70^\circ\text{N}$  and  $155^\circ\text{E}$ – $130^\circ\text{W}$  (He et al., 2012).

The wintertime (December–January–February) back trajectories of airflows were calculated by using the NOAA Hybrid Single-Particle Lagrangian Integrated Trajectory (HYSPLIT) model ([https://ready.arl.noaa.gov/HYSPLIT\\_traj.php](https://ready.arl.noaa.gov/HYSPLIT_traj.php)) (Rolph et al., 2017; Stein et al., 2015). Air temperature, three-dimensional wind, precipitation, geopotential height, and relative humidity from the National Centers for Environmental Prediction–National Center for Atmospheric Research reanalysis were used as the input data. The 72-hour back trajectories were performed every 6 h with a 1-hour time interval on 500 m altitude for 2004/05–2015/16. The altitude was selected to trace back the air masses entering below the boundary layer height in winter (Choi et al., 2008; Lee and Kim, 2018; Park and Lee, 2015). Four—Seoul ( $37.54^\circ\text{N}$ ,

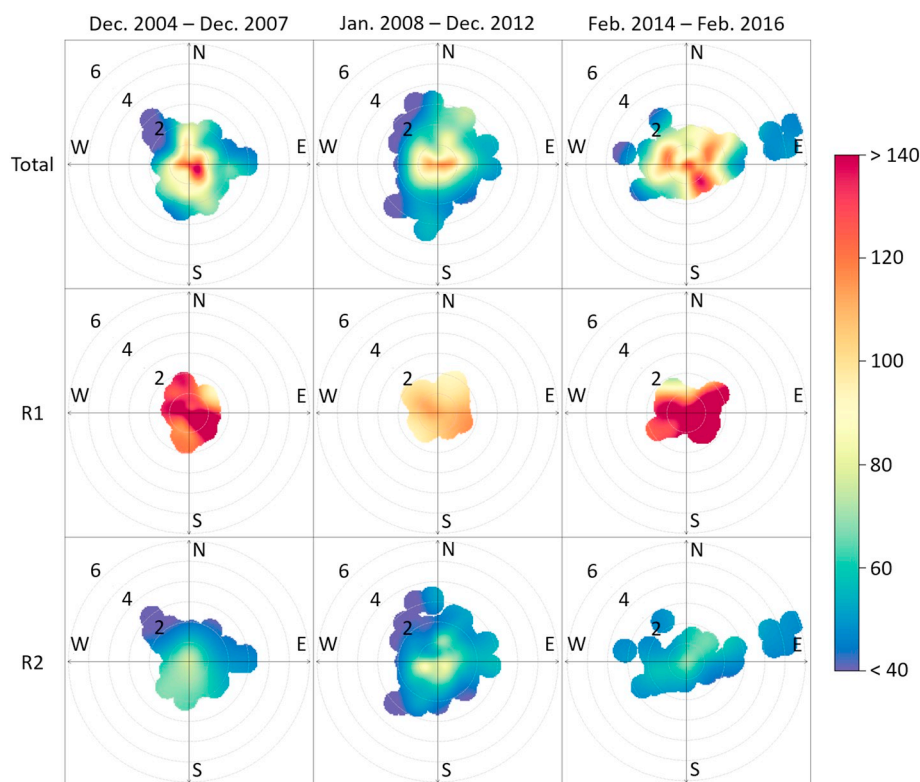


Fig. 5. Bivariate polar plots of winter  $PM_{10}$  concentrations ( $\mu\text{g m}^{-3}$ ) as functions of the wind direction and wind speed. R1 and R2 regions include stations with the largest and smallest eigenvectors (upper and lower 30%, i.e., 19 regions each), respectively, of the first EOF mode (Fig. 2a). Numbers over the circles depict wind speed ( $\text{m s}^{-1}$ ).

126.99°E), Busan (35.16°N, 129.06°E), Gwangju (35.17°N, 126.87°E), and Jeju (33.50°N, 126.52°E)—out of 10 cities were selected as starting points to evaluate the results according to the location of the cities.

The Potential Source Contribution Function (PSCF) method (Ashbaugh et al., 1985; Zeng and Hopke, 1989) was used to estimate the probable source regions. The PSCF value of a grid is defined as the ratio of the number of endpoints (i.e., the positions of the air parcels at each time increment) that correspond to observed concentration values greater than a given threshold, to the total number of endpoints within the grid, as Eq. (5),

$$PSCF_{ij} = \frac{m_{ij}}{n_{ij}} \quad (5)$$

where  $m_{ij}$  is the number of endpoints in the  $ij^{\text{th}}$  grid that corresponds to the observed concentration value higher than a threshold, and  $n_{ij}$  is the total number of endpoints in the grid. In this study,  $80 \mu\text{g m}^{-3}$ , a criterion for defining air quality with respect to  $PM_{10}$  concentration as “bad” in South Korea, was used as the threshold. The PSCF values were calculated in  $25^{\circ}\text{N}$ – $85^{\circ}\text{N}$ ,  $45^{\circ}\text{E}$ – $170^{\circ}\text{E}$  for each  $1^{\circ}$  resolution grid cell. To filter out source regions with extremely high probabilities due to small  $n_{ij}$ , an arbitrary weight function  $W$  were multiplied to the PSCF values (Hwang and Hopke, 2007; Polissar et al., 2001):

$$W = \begin{cases} 1.0 & 3N < n_{ij} \\ 0.7 & 1.5N < n_{ij} \leq 3N \\ 0.4 & N < n_{ij} \leq 1.5N \\ 0.2 & 0 < n_{ij} \leq N \end{cases} \quad (6)$$

where  $N$  is the average of  $n_{ij}$  in all grids.

To group the back trajectories on high- $PM_{10}$  days ( $>80 \mu\text{g m}^{-3}$ ) into several inflow patterns, an agglomerative hierarchical clustering algorithm based on the Euclidean distance measure and the Ward’s minimum variance clustering criterion were applied (Lee et al., 2011).

The longitudes and latitudes of the back trajectories with a 1-hour time interval were used as clustering variables. The number of clusters was determined as four by assessing the occurrence of noticeable increases in the distances between merged clusters with regards to four cities (Seoul, Busan, Gwangju, and Jeju) in South Korea.

### 3. Results

#### 3.1. Two leading EOF modes of $PM_{10}$ concentrations

Our investigation is focused on the spatiotemporal variations of winter  $PM_{10}$  concentrations over East Asia in 2004/05–2015/16 (Fig. 1). The mean concentrations in South Korea are about  $50 \mu\text{g m}^{-3}$  in central areas such as Seoul, Incheon, and Daegu (a basin terrain surrounded by mountains); below  $50 \mu\text{g m}^{-3}$  in other regions (Fig. 1a). In China, the mean concentrations are between 100 and  $150 \mu\text{g m}^{-3}$  in most regions except for the southern and coastal regions and are over  $150 \mu\text{g m}^{-3}$  in areas of similar latitudes as South Korea. As shown in Fig. 1b, the time series of the area average for South Korea shows that the concentration decreases more gradually than in China until 2012—the slopes ( $p$ -values) of the area averages in South Korea and China are  $-0.27 \mu\text{g m}^{-3} \text{ month}^{-1}$  (0.21) and  $-1.14 \mu\text{g m}^{-3} \text{ month}^{-1}$  (0.01), respectively. From January 2013 to February 2016, the slope ( $p$ -value) in South Korea is  $-0.70 \mu\text{g m}^{-3} \text{ month}^{-1}$  (0.16), indicating increases in  $PM_{10}$  concentrations right after 2013 and thereafter decreases in them. The domain average concentration in China decreases until 2012, then increases abruptly in 2014 and 2015 with relatively large fluctuations compared to South Korea—the slopes ( $p$ -values) after February 2014 in South Korea and China are  $-0.34 \mu\text{g m}^{-3} \text{ month}^{-1}$  (0.71) and  $-4.81 \mu\text{g m}^{-3} \text{ month}^{-1}$  (0.07), respectively. The time series of AOT (Fig. S3) and  $PM_{2.5}$  concentrations observed by the US Department of State (Fig. S4) also show an abrupt worsening of air quality in most regions of China during 2013–2015.

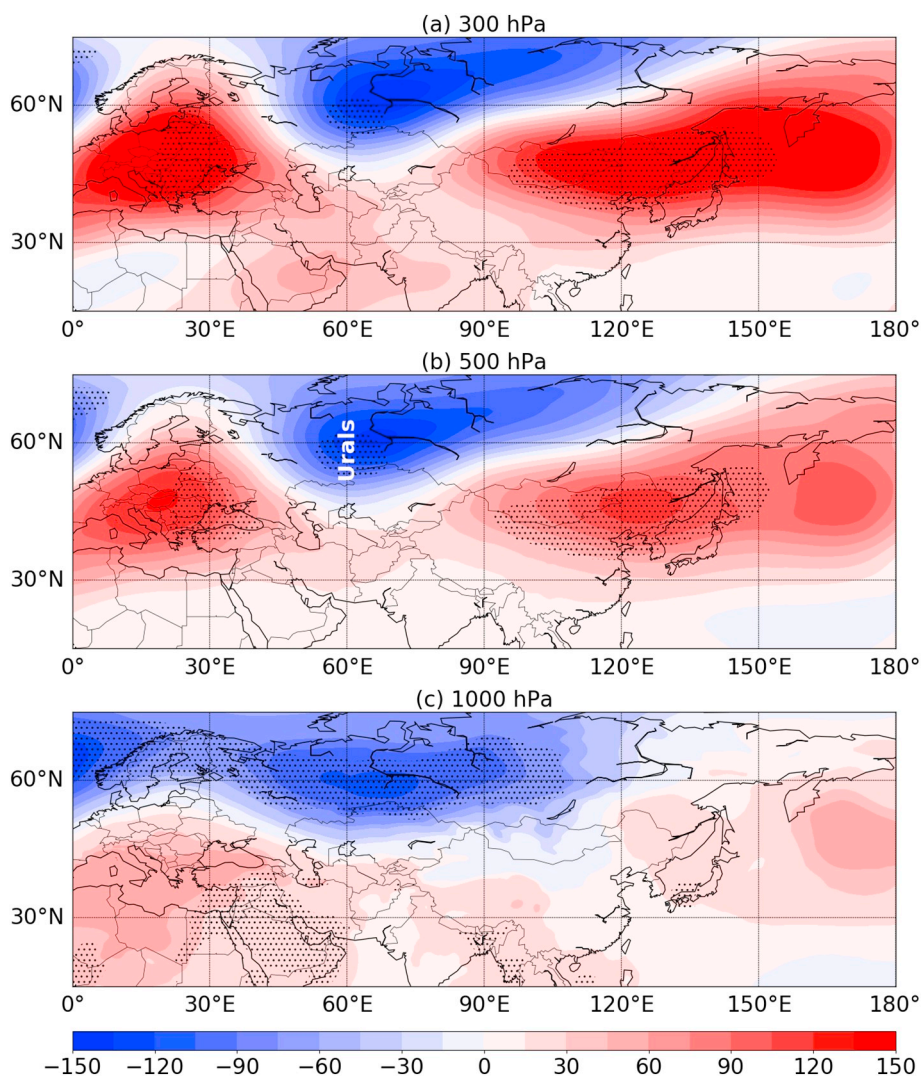


**Fig. 6.** Differences (the third minus the second sub-period) of composite geopotential height anomalies (gpm) at (a) 300, (b) 500, and (c) 1000 hPa between three months in the third sub-period (February 2014, January and December 2015) and four months in the second sub-period (February 2010, January 2011, February and December 2012) in which the absolute values of Fig. 2b are greater than  $1\sigma$ . The dots indicate that the value is significant at the 95% confidence level. The coordinates of the Ural Mountains are (60°N, 60°E).

To identify the dominant spatiotemporal variability of air quality, an EOF analysis is performed for  $PM_{10}$  concentrations over East Asia. Fig. 2a and b show that the most dominant mode of variability in the monthly mean  $PM_{10}$  anomalies, characterized by a decrease until 2012 and an increase in 2014 and 2015, accounts for 32.7% of the total variance with nearly identical interannual variations over East Asia, especially in eastern and northeastern China. The peak value of the first EOF mode in February 2014 reflects rises in  $PM_{10}$  concentrations due to frequent severe haze episodes during the month (Li et al., 2016; Yan et al., 2015). Fig. 2c and d show that the second EOF mode, characterized by a decreasing trend over the entire analysis period, accounts for 20.1% of the total variance. The corresponding spatial pattern features positive anomalies in most regions of South Korea except Jeju, and in northeastern and central China; negative anomalies occur over eastern China, e.g., the Shandong province.

The variations in large-scale atmospheric circulations clearly affect the variability of aerosol concentrations over a large region. To emphasize the effect of the atmospheric control mechanisms on  $PM_{10}$  concentrations over East Asia, the EOF analysis is performed to

detrended  $PM_{10}$  concentrations; this essentially removes the second EOF mode which represents the variability associated with the long-term linear trend (not shown). The first EOF mode covers 39.8% of the total variance with a spatial pattern and the time series similar to those in Fig. 2a and b, respectively; the correlation coefficients calculated for the eigenvectors and principal components between Fig. 2a and b and those from the EOF analysis of detrended  $PM_{10}$  concentrations are 0.99. The leading mode is distinguished well (North et al., 1982) from the remaining modes which show random patterns. Based on this additional analysis, the first EOF time series (Fig. 2b) is used as the reference for the regression analysis of the atmospheric variables. If the increases in  $PM_{10}$  concentrations in 2014 and 2015 can be explained by the atmospheric fields related to the EOF mode, mechanisms for the recent changes in  $PM_{10}$  concentrations over East Asia can be identified.

### 3.2. Regressed atmospheric patterns with respect to the two leading EOF time series

To identify key factors that drive the changes in winter  $PM_{10}$

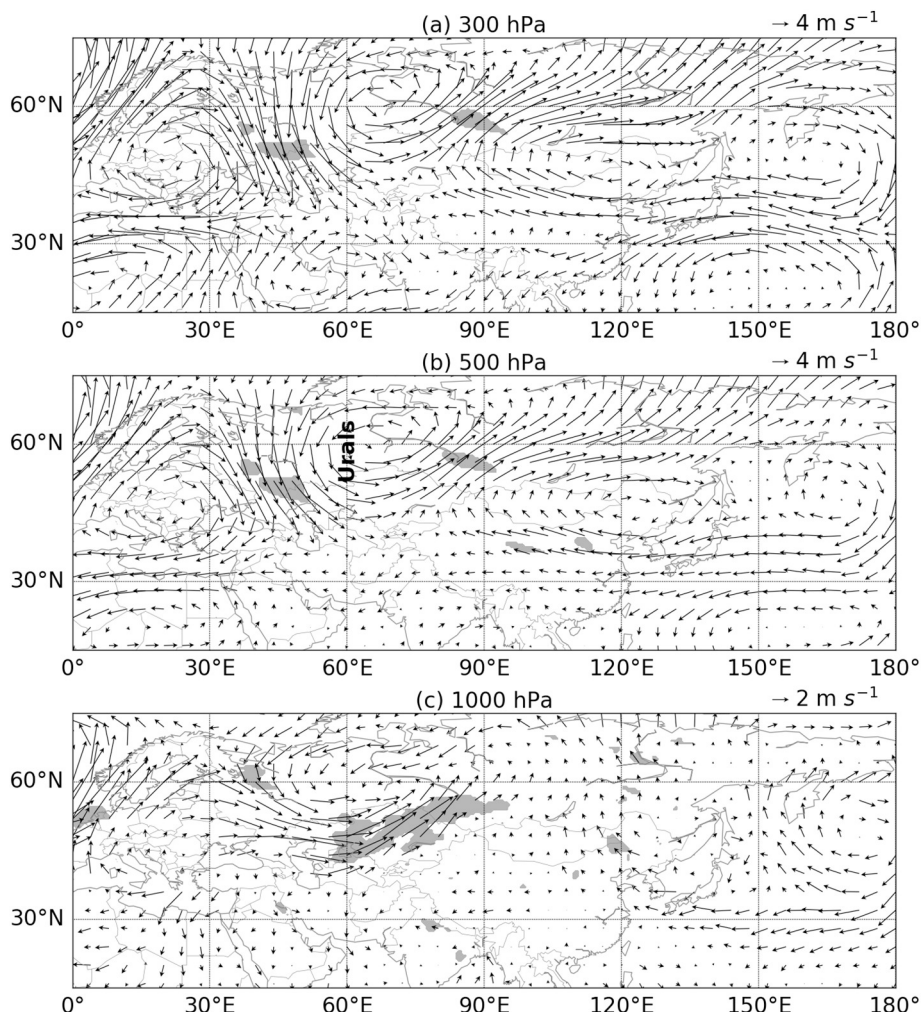
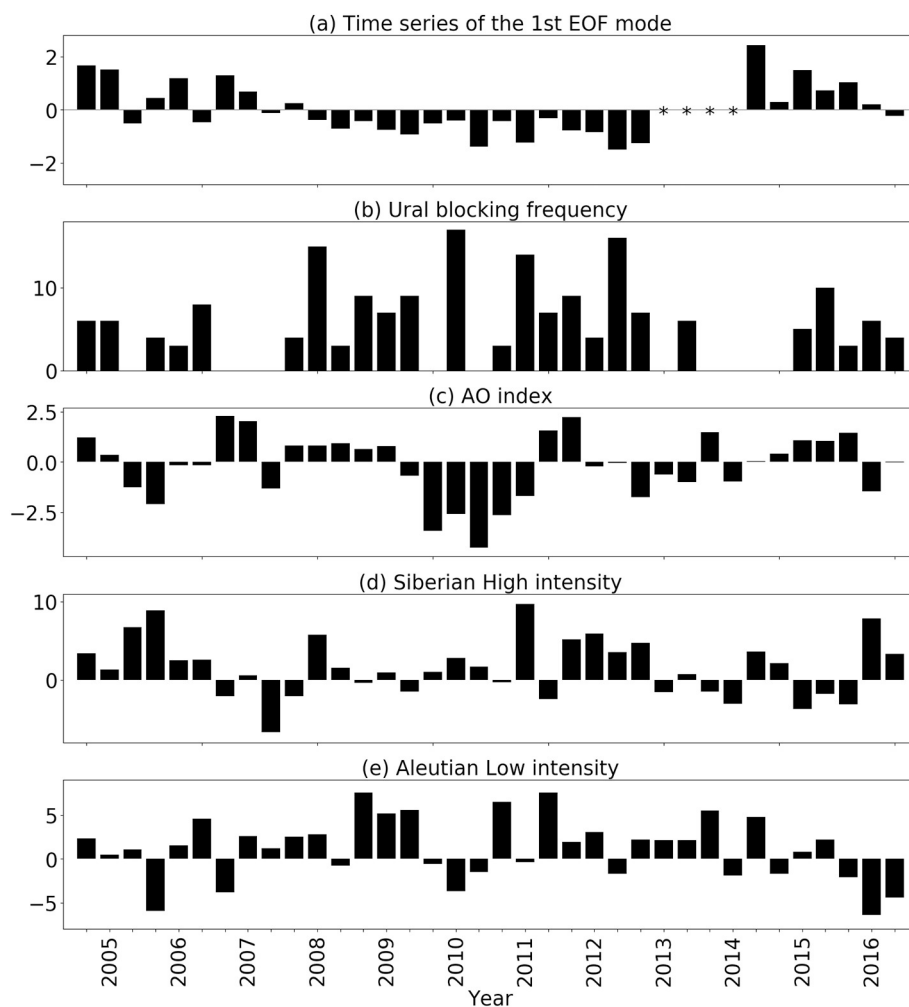


Fig. 7. The same as that shown in Fig. 6 except for wind anomalies ( $\text{m s}^{-1}$ ). The shades indicate that the value is significant at the 95% confidence level. The coordinates of the Ural Mountains are ( $60^\circ\text{N}$ ,  $60^\circ\text{E}$ ).

concentrations in East Asia, regression analysis of the atmospheric variables with respect to the first EOF time series (Fig. 2b) is conducted. Overall, the 300, 500, and 1000 hPa regressed geopotential heights are characterized by a barotropic structure (Fig. 3). The pattern is more pronounced in higher levels, implying a relationship between the interannual variability of  $\text{PM}_{10}$  concentrations and large-scale atmospheric circulations. The negative anomalies in the 500-hPa level over the region to the east of the Ural Mountains (Fig. 3b) indicate the weakening of the Ural blocking. The positive anomalies over northern Korea and China in the middle troposphere imply the weakening of the East Asian trough, one of the indicators for weak EAWM (Wu et al., 2006). The weakened Ural blocking and East Asian trough lead to weaker cold air transports from Siberia towards the south into Korea and China (Chang et al., 2016). The anomalies in the lower troposphere (Fig. 3c) show weaker Siberian High and East Asian trough. The regressed wind vectors at the same three levels characterized by easterlies (Fig. 4a and b) and southeasterlies (Fig. 4c) over Korea and China indicate the weakening of westerlies and northwesterlies in response to the weaker East Asian trough, leading to poor ventilation effects and the deterioration of air quality in the region as found in previous studies (Kim et al., 2017b; Shi et al., 2019). The intensification of the polar jet around  $60^\circ\text{N}$  on the 300-hPa level (Fig. 4a), related to the restraint in the blocking events over the Ural region (He and Wang, 2016), also

prevents the cold air inflows from the north, eventually leading to the degradation of air quality in East Asia.

The resulting accumulation of air pollutants due to poor ventilation is shown in the bivariate polar plots of regional transport patterns (Fig. 5). Notice that this plot represents how  $\text{PM}_{10}$  concentrations vary together with wind speed and direction in polar coordinates. Here, the whole analysis period is divided into three sub-periods (December 2004–December 2007, January 2008–December 2012, and February 2014–February 2016) with respect to the signs of the first EOF time series (see Fig. 2b). The bivariate polar plots over the entire region show that high  $\text{PM}_{10}$  concentrations are associated with weak winds and that the concentrations are higher in the first and third sub-periods compared to the second sub-period. High concentrations are associated with larger easterly wind anomalies in the third sub-period compared to the first sub-period. In the R1 regions where eigenvectors of the first EOF mode are in the upper 30% (red-squared regions in Fig. 2a), mostly in eastern and northeastern China, high  $\text{PM}_{10}$  concentrations are associated with weak winds for the entire period.  $\text{PM}_{10}$  concentrations are higher in the first and third sub-periods than in the second sub-period. The close association of high  $\text{PM}_{10}$  concentrations with the easterly wind anomalies in the third sub-period suggests that the lack of ventilation associated with large-scale atmospheric circulations is critical in generating high  $\text{PM}_{10}$  concentration events in East Asia after 2014.



**Fig. 8.** (a) The same as Fig. 2b, (b) the Ural blocking frequency (days), (c) the AO index, (d) the Siberian High intensity (hPa), and (e) the Aleutian Low intensity (hPa).

The differences of geopotential heights and winds between the third and the second sub-periods (the third minus the second sub-period; Figs. 6 and 7) also show the weakening of the Ural blocking and westerlies over East Asia, and therefore imply the reduced ventilation. The mean Ural blocking frequencies (Fig. 8b) in the second and the third sub-periods are 8 and 4 days, respectively, indicating the weakening of the Ural blocking in the third sub-period as well. The worsened air quality in these regions associated with large-scale atmospheric circulation and local meteorological conditions, in spite of the national efforts to reduce the emissions, suggests that stronger emission reduction goal has to be established. In the R2 regions including South Korea and coastal China where the eigenvectors of the first EOF mode are in the lower 30% (blue-squared regions in Fig. 2a), low  $PM_{10}$  concentrations and strong winds occur for the entire period. The variations in  $PM_{10}$  concentrations in each sub-period can also be found in the time series of  $PM_{10}$  concentrations in two regions R1 and R2 (Fig. S5). The concentration in R1 is high in the first, low in the second, and high in the third sub-period, similar to the domain average in China; the concentration in R2 does not show reliable temporal change.

Regression analysis of the remaining atmospheric variables with respect to the first EOF time series is conducted to identify the cause of the weakening of the Ural blocking (Fig. 9). Firstly, the surface air temperature anomalies (Fig. 9a) are positive over East Asia, and thus

the increases in  $PM_{10}$  concentrations is unlikely to be caused by increased emissions from additional space heating (Chen et al., 2013a; Xiao et al., 2015). Also, Cheung et al. (2012) and He and Wang (2016) demonstrated that the Ural blocking frequency after the positive phase of AO becomes small, which is a favorable condition for warm conditions in East Asia. The weakened Ural blocking, positive surface air temperature anomalies over East Asia, and mostly positive AO indices after 2014 (Fig. 8c) correspond to the mechanism to induce bad air quality as found in previous studies. In addition, positive/negative surface air temperature anomalies occur in the south/north of the area where the polar jet is located, indicating larger temperature gradients and thus intensification of the polar jet; this is consistent with the pattern in Fig. 4a.

Secondly, sea surface temperature in the North Atlantic can also be remotely related to the Ural blocking. Li (2004) revealed that the sea surface temperature anomaly is linearly linked to the wave-train-like height anomaly chain, resulting in a geopotential height anomaly over the Urals. Han et al. (2011) explained that the sea surface temperature anomaly induces blocking high over the Urals through anomalous transient eddies. Sea surface temperature shows negative anomalies in the northern North Atlantic (Fig. 9b), which indicate the weak energy transformation from the transient eddies to the wave-like low-frequency variability over the domain from the north Atlantic to the Urals,

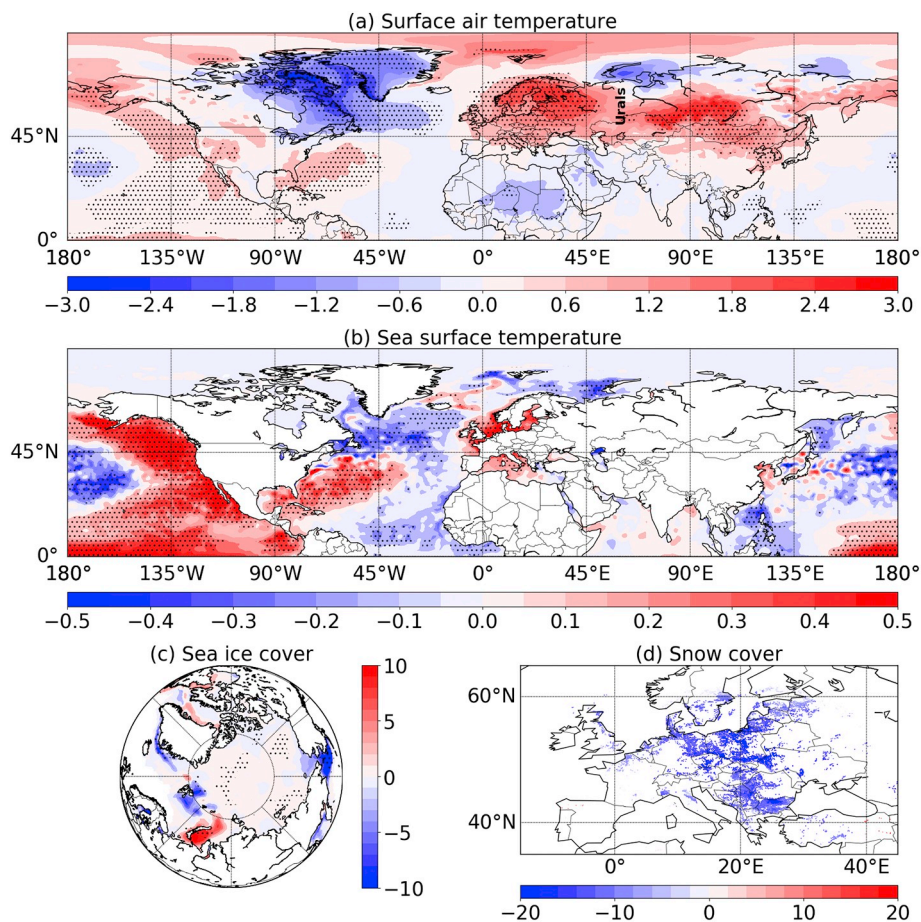


**Fig. 9.** The same as that shown in Figs. 3 and 4 except for (a) surface air temperature ( $^{\circ}\text{C}$ ), (b) sea surface temperature ( $^{\circ}\text{C}$ ), (c) sea ice cover (%), and (d) snow cover (%) anomalies. The dots in (a)–(c) indicate that the value is significant at the 95% confidence level. The coordinates of the Ural Mountains are ( $60^{\circ}\text{N}$ ,  $60^{\circ}\text{E}$ ).

and thus the reduced maintenance of the Ural blocking by the weak transient-eddy forcing.

Thirdly, sea ice cover in the Barents-Kara Seas can affect the Ural blocking (Luo et al., 2016; Yao et al., 2017). Warming of the Barents-Kara Seas favors sea ice loss in these regions which in turn reduces the meridional temperature gradient. The resulting weakening of westerlies and vertical shear over the mid- and high-latitude Eurasian region is favorable for increasing the persistence of Ural blocking events. Fig. 9a and c show negative anomalies of surface air temperatures and positive anomalies of sea ice cover over the Kara Sea, which can induce an increase in the meridional temperature gradient, the strengthening of westerlies and vertical shear, and the weakening of the persistence of Ural blocking. Thus, the regressed patterns of sea ice and surface air temperatures, as opposed to the previous studies, may have affected the weakening of the Ural blocking.

Finally, positive/negative anomalies of the surface air temperatures/snow cover in Europe can modulate the intensity of the Ural blocking (Fig. 9a and d). He and Wang (2016) and Zhou et al. (2009) revealed that the surface warming in this region due to reduced surface albedo by enhanced snowmelt may stimulate a Rossby wave train to propagate eastward across Eurasia; such wave-mean flow interaction may restrain blocking events around the Ural region. Further studies on the relationship between geopotential height/wind and surface air temperature/snow cover are needed because the causality can be controversial: Chen et al. (2016) suggested that surface wind anomalies associated with atmospheric circulation may contribute the formation

of surface air temperature anomalies and snowmelt over Eurasia. In summary, the weakening of the Ural blocking after 2014 is attributable to the positive phase of AO, a decrease in sea surface temperature in the northern North Atlantic, an increase in sea ice cover over the Kara Sea, and a decrease in snow cover in Europe.

In contrast to the aforementioned results, the regressed geopotential heights and winds relative to the second EOF time series (Fig. 2d) do not show any noteworthy features (Figs. 10 and 11, respectively). Instead of large-scale atmospheric circulations, the pattern of the second EOF mode resembles the linear trends of  $\text{PM}_{10}$  concentrations (Fig. 12) with a correlation coefficient of 0.97. Thus, the second EOF mode can be a reflection of the decreases/increases in  $\text{PM}_{10}$  concentrations due to the changes in air pollutant emissions by the implementation of reduction policies in South Korea and China. The minimum and maximum values of the linear slopes in South Korea are  $-0.76$  and  $0.07 \mu\text{g m}^{-3} \text{ month}^{-1}$ , respectively; those in China are  $-4.18$  and  $3.37 \mu\text{g m}^{-3} \text{ month}^{-1}$ , respectively. We note that the large increases in  $\text{PM}_{10}$  concentrations near the Shandong province can be closely related to the increasing fossil fuel use and resulting air pollutant emissions as described in previous studies (Fan and Wang, 2016; Sun et al., 2016; Zhang et al., 2017; Zhang et al., 2018a). Sun et al. (2016) stated that the total  $\text{PM}_{10}$  emissions from the Shandong vehicle fleet have increased from 12.4 Gg in 2000 to 29.5 Gg in 2014 because of a sharp growth in the number of vehicles in recent years. Zhang et al. (2018a) reported that the coal consumption in the Shandong province continued to increase from 2011 to 2015 mainly because of the growth in the high-

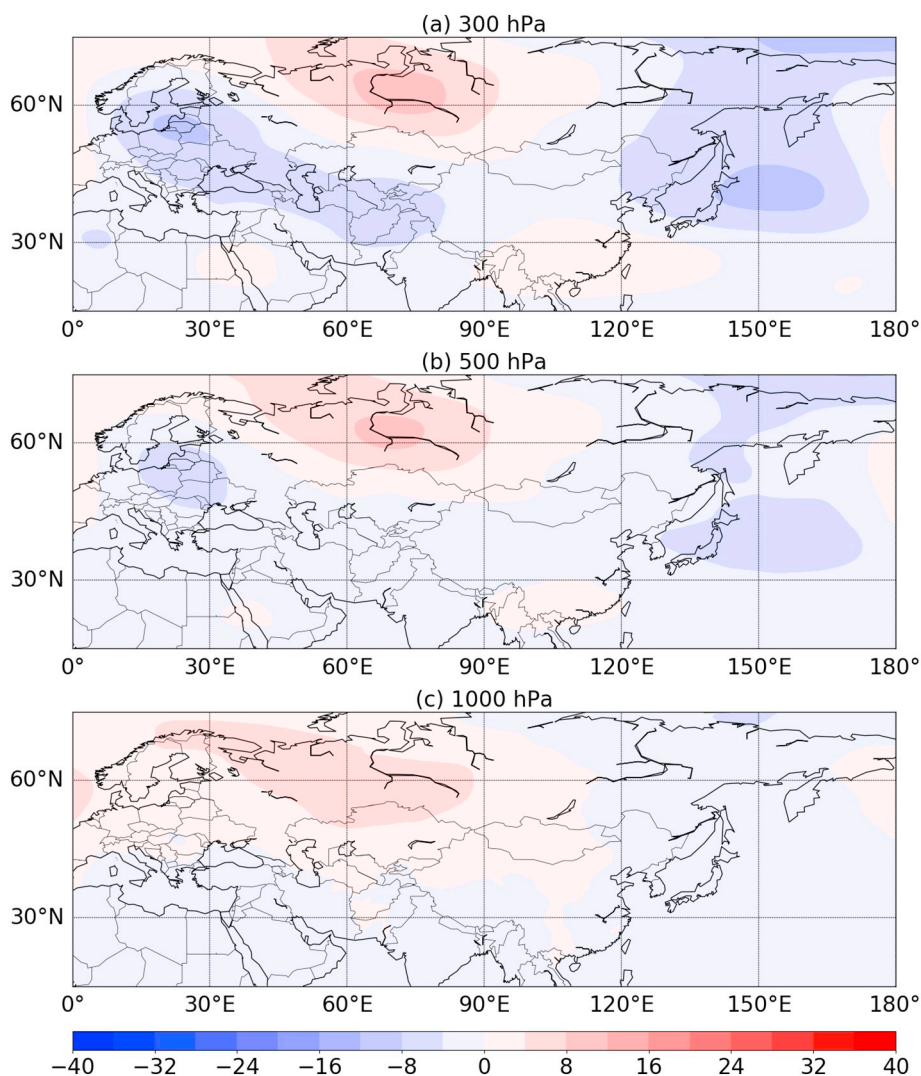


Fig. 10. The same as that shown in Fig. 3 except for the second EOF time series.

coal-consumption industry, in contrast to other regions in China where coal consumption has been decreasing since 2013. The increased air pollutant emissions associated with economic growths in China appear to offset the emission reduction under stringent regulations.

Our findings emphasize that the long-term variability of  $PM_{10}$  concentrations in East Asia can be explained by considering the variations in large-scale atmospheric circulations as well as the emissions of air pollutants. This study also suggests that considering the effect of large-scale atmospheric circulations on local air quality, and thus the consideration of long-term climate variability, is essential when establishing long-term air quality policies.

#### 4. Discussion

Figs. 2c and 12 showed that the second EOF mode is a reflection of the linear trends of  $PM_{10}$  concentrations in East Asia. In order to discuss the variability of air quality in China, not only the long-term trends but also the differences in  $PM_{10}$  concentrations by regions and time slices need to be analyzed because of different emission sources, geographic properties, the content of clean air policies, and the timing of the implementation of policies from region to region. Fig. 13 shows the  $PM_{10}$  concentration differences between the first and the second sub-periods

(the second minus the first; Fig. 13a) and the second and the third sub-periods (the third minus the second; Fig. 13b). The differences in  $PM_{10}$  concentrations between the first and second sub-periods occurred in northeastern China, while the differences between the second and third sub-periods appear in eastern and northeastern China, near the Yellow Sea. The location of these regions is also similar to the central heating area—the northern part of the Huai River and Qin Mountains (Chen et al., 2013a; Xiao et al., 2015). It suggests that, if meteorological conditions in regions with high air pollutant emissions are stagnated due to the effects of atmospheric circulation, regional air quality can be deteriorated abruptly despite the national efforts to reduce the emissions. In addition, during the third sub-period,  $PM_{10}$  concentrations in eastern China in 2015 increased from the 2014 level, while those in northeastern and central China decreased (Fig. S6a). In 2016, the concentrations decreased from the 2015 level in most regions (Fig. S6b), which coincides with the previous findings (Chen et al., 2018; Yang et al., 2018). The domain average of  $PM_{10}$  concentrations in China is  $126.74 \mu\text{g m}^{-3}$ ,  $130.05 \mu\text{g m}^{-3}$ , and  $107.02 \mu\text{g m}^{-3}$  in 2014, 2015, and 2016, respectively. The concentration decreased in 2016, yet the value itself is still high. It is noted that the concentration decreased in both 2015 and 2016 over northeastern China, whereas it increased in 2015 and then decreased in 2016 over eastern China, indicating

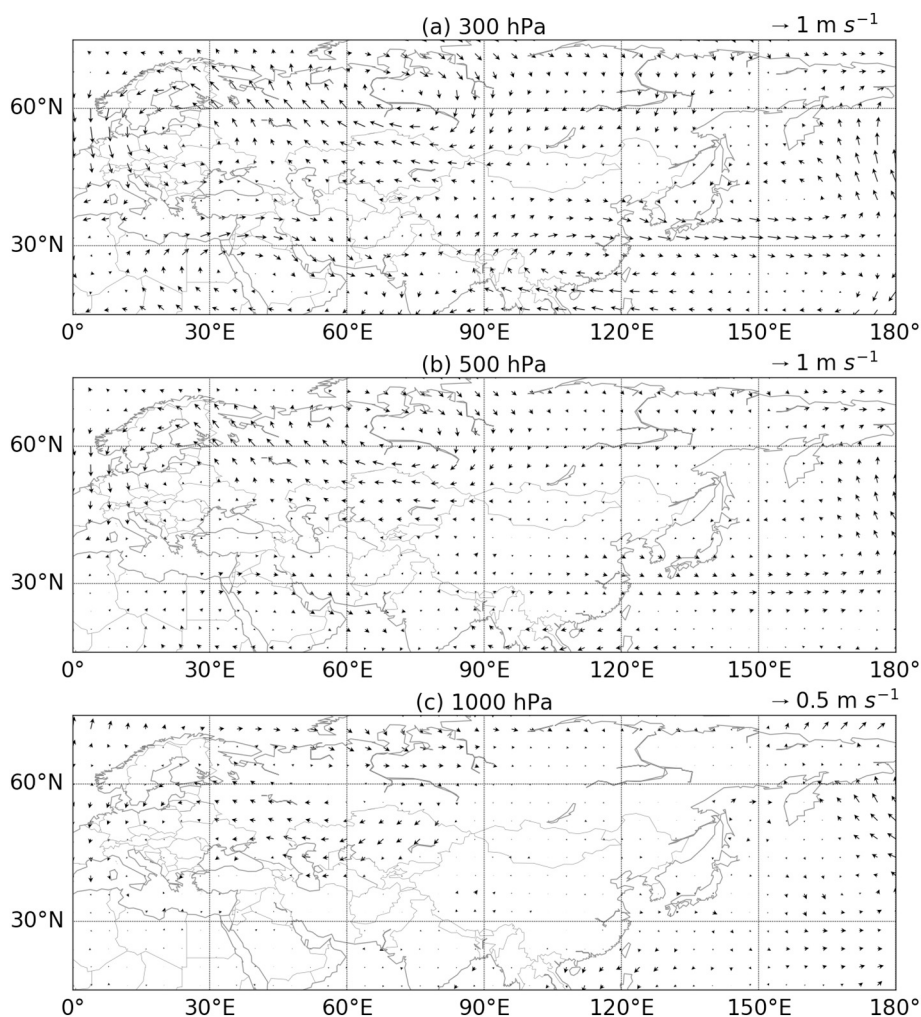


Fig. 11. The same as that shown in Fig. 4 except for the second EOF time series.

relatively small concentration reduction compared to that over north-eastern regions. Since large-scale atmospheric circulations and local meteorological conditions can increase  $PM_{10}$  concentrations abruptly, the reduction of air pollutant emissions needs to be accelerated, considering that air quality can get worse in the future under similar atmospheric conditions in 2014 and 2015.

In Fig. 2, the absolute values of eigenvectors in South Korea were relatively smaller than those in China due to lower  $PM_{10}$  concentrations. Nonetheless, the present results are also significant for analyzing long-term variability of air quality in South Korea because  $PM_{10}$  concentrations over the region can be influenced by both transboundary transport of air pollutants from China and atmospheric circulations affecting air quality in China, because the two countries are geographically close. As South Korea is located in the east of the Shandong province, it may be assumed that the variability of  $PM_{10}$  concentrations is similar to that in the Shandong province. Jeong et al. (2017) revealed that air quality in Seoul, South Korea is critically modulated by the transboundary transport of air pollutants from the Shandong province for all seasons. However, the results for winter were rather different—the trends in South Korea were negative, unlike the positive trends in the Shandong province (Fig. 12). The spatial distributions of the PSCF values and mean back trajectories of major clusters (Fig. 14 and

Table 1) show that the probable source regions during winter include Beijing-Tianjin-Hebei, the Yangtze River Delta, and Inner Mongolia as well as the Shandong province. These results imply that air pollutant emissions in various source regions in eastern and northeastern China contribute to bad air quality episodes in South Korea during winter; that is, the  $PM_{10}$  concentration trend in South Korea would be different from that in the Shandong province.

In this study, we have focused on the effect of the Ural blocking on wintertime  $PM_{10}$  concentrations in East Asia. However, other large-scale factors can also affect air quality in East Asia as discussed in the Introduction. Variations in the Siberian High or the Aleutian Low, for instance, can induce adverse meteorological conditions to local air quality in East Asia (Oh et al., 2018; Zhao et al., 2018). Our results, however, do not identify any noticeable long-term variations in the intensity of the Siberian High and the Aleutian Low (Figs. 3, 8d, and e). The discrepancy in the results between the current study and previous ones may be partly due to the differences in the analysis period, considering that the factors affecting air quality vary from period to period. In order to identify the causality for the variations of aerosol concentrations in other periods, more of the reported factors that affect air quality in East Asia will be examined in the future.

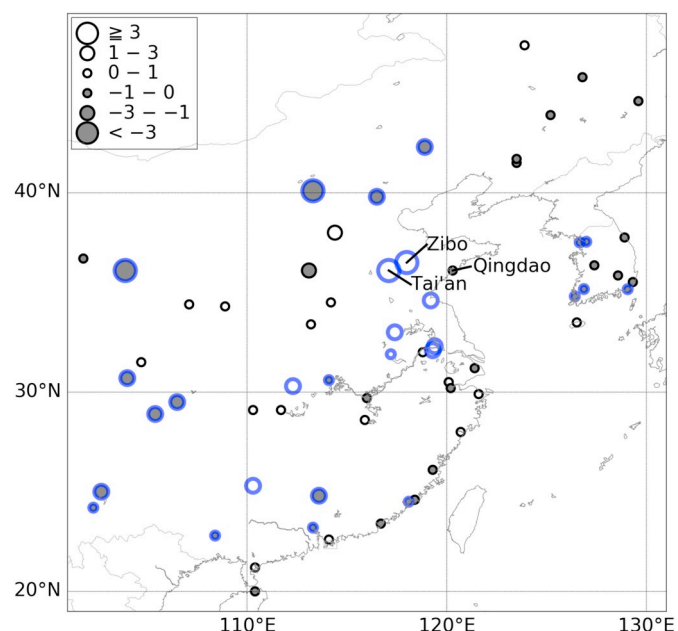


**Fig. 12.** Spatial distribution of the linear trend of wintertime (December–February) monthly-mean  $PM_{10}$  concentration over East Asia. The unit is  $\mu\text{g m}^{-3} \text{ month}^{-1}$ . The blue circles indicate that the trend is significant at the 95% confidence level. Qingdao, Tai'an, and Zibo are located in Shandong province. (For interpretation of the references to colour in this figure legend, the reader is referred to the web version of this article.)

## 5. Summary

Wintertime  $PM_{10}$  concentrations in South Korea and China have decreased since the 2000s as the implementation of strict air quality regulations. The decreasing trend, however, has been slowed down or even reversed in recent years. We have analyzed the dominant modes of the variations in winter  $PM_{10}$  concentrations observed in the two countries using an EOF analysis to identify the atmospheric mechanisms behind the changes in  $PM_{10}$  concentrations during the period 2004/05–2015/16. The first EOF mode accounts for 32.7% of the total variance with a decrease until 2012 and then an increase in 2014 and 2015. The regression analysis with respect to the first EOF time series indicates that the variability of winter  $PM_{10}$  concentrations in East Asia is related to the Ural blocking which has weakened after 2014 because of the positive phase of AO, a decrease in sea surface temperature in the northern North Atlantic, an increase in sea ice cover over the Kara Sea, and a decrease in snow cover in Europe. When the Ural blocking is weakened, the northerly transports of cold air into Korea and China are hindered, causing favorable conditions for accumulating air pollutants in East Asia. The second EOF mode accounts for 20.1% of the total variance and shows a similar spatial distribution to the linear trend of  $PM_{10}$  concentrations.

One of the most influencing causes of bad air quality episodes in East Asia is the large-scale control mechanism that induces adverse local meteorological conditions. Analyzing  $PM_{10}$  concentrations together with atmospheric circulations, this study suggests that the weakening of the Ural blocking can affect the increases in winter  $PM_{10}$  concentrations over East Asia. Our results also imply that, despite all the efforts to tackle air pollution, an unexpected deterioration of air quality can occur concurrently with the implementation of reduction policies under certain atmospheric conditions; thus, in order to prevent similar worsening of air quality, countries that still emit a large amount of air pollutants are required to set the emission reduction goal

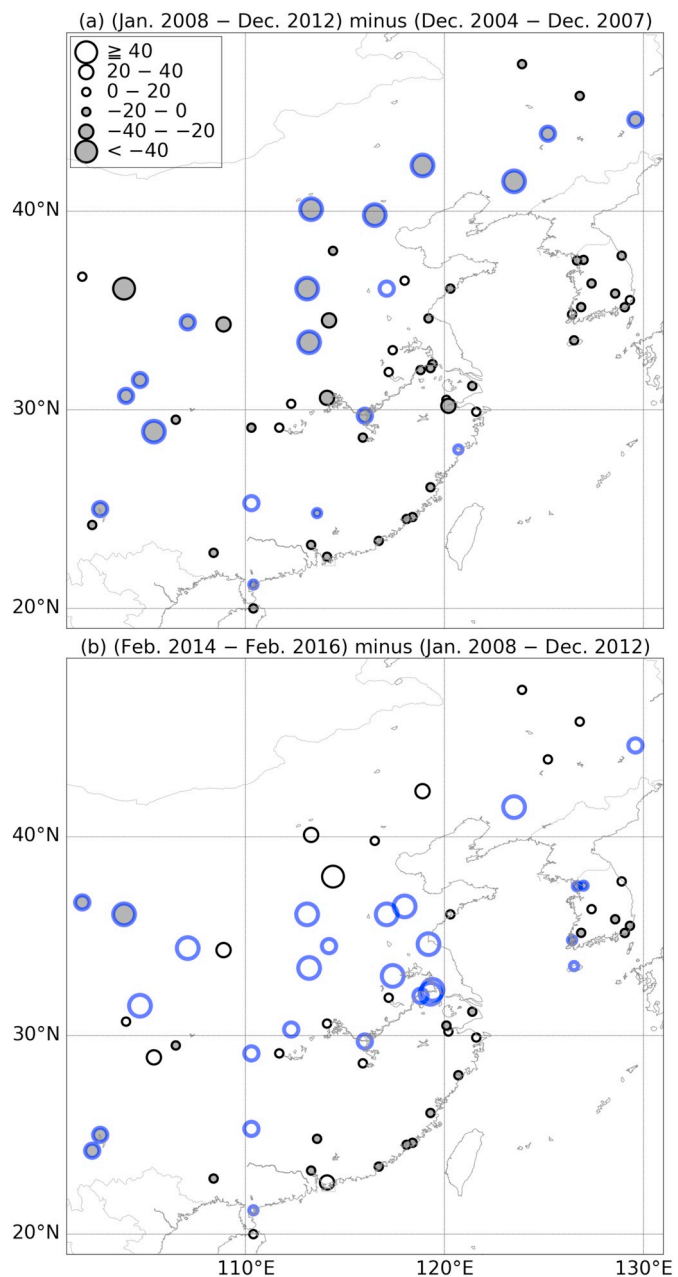


**Fig. 13.** Differences of winter (December–February)  $PM_{10}$  concentrations ( $\mu\text{g m}^{-3}$ ) between (a) the first and the second (the second minus the first) sub-period, and (b) the second and the third (the third minus the second) sub-period. The blue circles indicate that the difference is significant at the 95% confidence level. (For interpretation of the references to colour in this figure legend, the reader is referred to the web version of this article.)

stronger, even if the emissions are being lowered currently. The present findings highlight the necessity of considering the relationship between air quality and large-scale atmospheric circulations as well as local emissions in establishing long-term air quality policies.

## Declaration of Competing Interest

The authors declare that they have no known competing financial interests or personal relationships that could have appeared to influence the work reported in this paper.

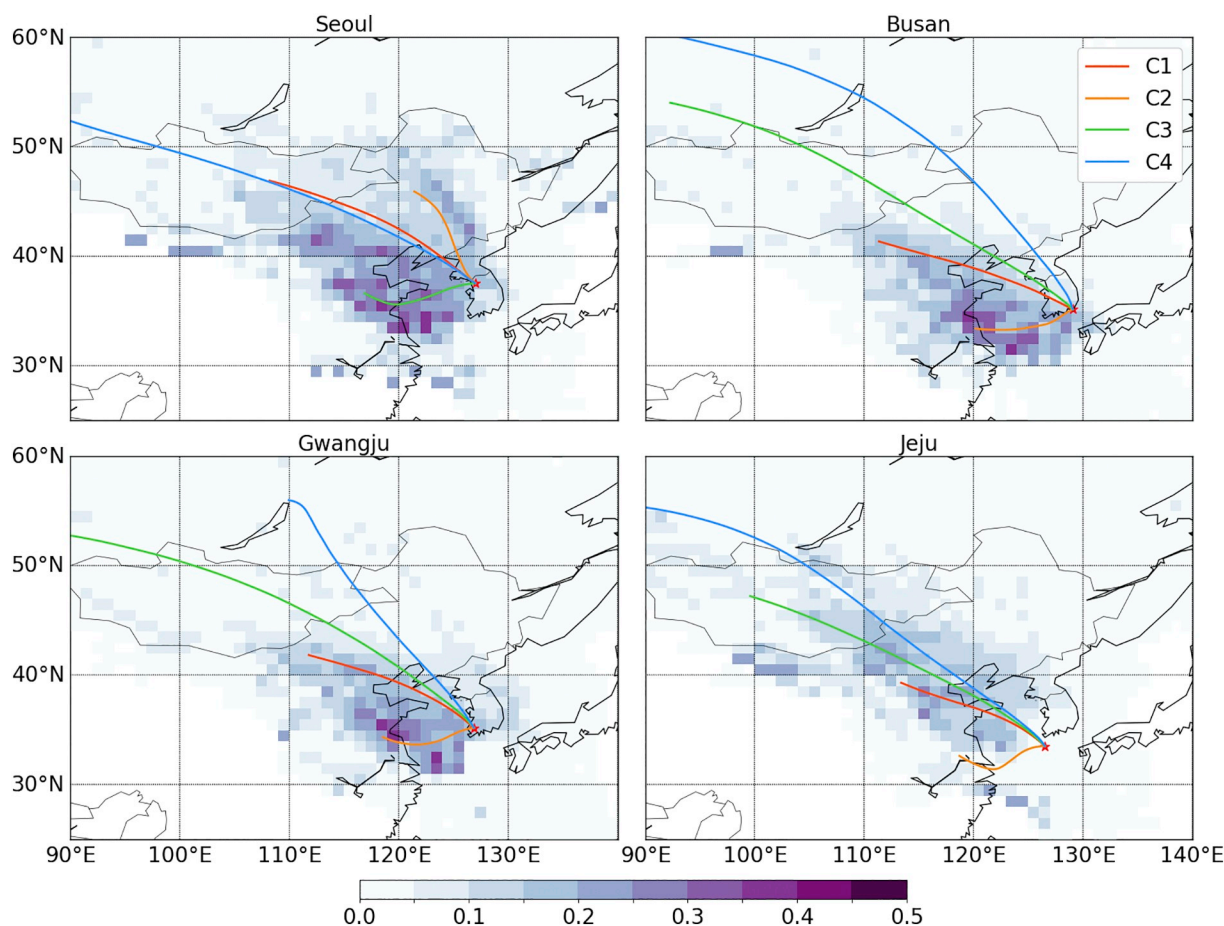


Fig. 14. PSCF maps of  $PM_{10}$  and mean back trajectories of four clusters for Seoul, Busan, Gwangju, and Jeju from 2004/05 to 2015/16. The proportion of back trajectories corresponding to C1 is the highest, followed by C2, C3, and C4 (Table 1).

Table 1

The ratio of the number of trajectories corresponding to each cluster to the total number of trajectories and the number of high- $PM_{10}$  days ( $> 80 \mu g m^{-3}$ ).

		Seoul	Busan	Gwangju	Jeju
Ratio	C1	0.34	0.60	0.55	0.53
	C2	0.27	0.26	0.29	0.22
	C3	0.26	0.13	0.09	0.17
	C4	0.13	0.02	0.06	0.08
High- $PM_{10}$ days		164	106	106	103

## Acknowledgments

This work was supported by the Korea Ministry of Environment (MOE) as “Climate Change Correspondence Program”. Seong-Joong Kim was supported by KPOPS project PE19130 of Korea Polar Research Institute.

## Appendix A. Supplementary data

Supplementary data to this article can be found online at <https://doi.org/10.1016/j.atmosres.2020.104871>.

## References

Ashbaugh, L.L., Malm, W.C., Sadeh, W.Z., 1985. A residence time probability analysis of sulfur concentrations at Grand Canyon National Park. *Atmos. Environ.* 19, 1263–1270.

Behara, S.N., Cheng, J.P., Huang, X., Zhu, Q.Y., Liu, P., Balasubramanian, R., 2015. Chemical composition and acidity of size-fractionated inorganic aerosols of 2013–14

winter haze in Shanghai and associated health risk of toxic elements. *Atmos. Environ.* 122, 259–271.

Chang, C.T., Tsai, C.J., 2003. A model for the relative humidity effect on the readings of the  $PM_{10}$  beta-gauge monitor. *J. Aerosol Sci.* 34, 1685–1697.

Chang, L., Xu, J., Tie, X., Wu, J., 2016. Impact of the 2015 El Niño event on winter air quality in China. *Sci. Rep.* 6, 34275.

Chen, Y., Ebenstein, A., Greenstone, M., Li, H., 2013a. Evidence on the impact of sustained exposure to air pollution on life expectancy from China’s Huai River policy. *Proc. Natl. Acad. Sci. U. S. A.* 110, 12936–12941.

Chen, C., Su, M.R., Liu, G.Y., Yang, Z.F., 2013b. Evaluation of economic loss from energy-related environmental pollution: a case study of Beijing. *Front. Earth Sci.* 7, 320–330.

Chen, G., Wang, Y., Li, S., Cao, W., Ren, H., Knibbs, L.D., Abramson, M.J., Guo, Y., 2018. Spatiotemporal patterns of  $PM_{10}$  concentrations over China during 2005–2016: a satellite-based estimation using the random forests approach. *Environ. Pollut.* 242, 605–613.

Cheung, H.N., Zhou, W., Mok, H.Y., Wu, M.C., 2012. Relationship between Ural–Siberian blocking and the East Asian winter monsoon in relation to the Arctic Oscillation and the El Niño–Southern Oscillation. *J. Clim.* 25, 4242–4257.

Chen, S., Wu, R., Liu, Y., 2016. Dominant modes of interannual variability in Eurasian surface air temperature during boreal spring. *J. Clim.* 29, 1109–1125.

Cheung, H.H.N., Zhou, W., Lee, S.-M., Tong, H.-W., 2015. Interannual and interdecadal variability of the number of cold days in Hong Kong and their relationship with large-scale circulation. *Mon. Weather Rev.* 143, 1438–1454.

China’s Ministry of Environmental Protection, 2012. Ambient Air Quality Standards (GB3095–2012). China Environmental Science Press, Beijing.

China’s Ministry of Environmental Protection, 2013. Technical Specifications for Installation and Acceptance of Ambient Air Quality Continuous Automated Monitoring System for  $PM_{10}$  and  $PM_{2.5}$  (HJ655–2013). China’s Ministry of Environmental Protection, Beijing.

Choi, H., Zhang, Y.H., Kim, K.H., 2008. Sudden high concentration of TSP affected by atmospheric boundary layer in Seoul metropolitan area during duststorm period. *Environ. Int.* 34, 635–647.

Cohen, A.J., Anderson, H.R., Ostra, B., Pandey, K.D., Krzyzanowski, M., Künzli, N., Gutschmidt, K., Pope, A., Romieu, I., Samet, J.M., Smith, K., 2005. The global burden of disease due to outdoor air pollution. *J. Toxic. Environ. Health A* 68, 1–7.

Dawson, A., 2016. eofs: A library for EOF analysis of meteorological, oceanographic, and climate data. *J. Open Res. Softw.* 4, e14.

Dee, D.P., Uppala, S.M., Simmons, A.J., Berrisford, P., Poli, P., Kobayashi, S., Andrae, U.,

- Balmaseda, M.A., Balsamo, G., Bauer, P., Bechtold, P., Beljaars, A.C.M., van de Berg, L., Bidlot, J., Bormann, N., Delsol, C., Dragani, R., Fuentes, M., Geer, A.J., Haimberger, L., Healy, S.B., Hersbach, H., Holm, E.V., Isaksen, I., Kallberg, P., Kohler, M., Matricardi, M., McNally, A.P., Monge-Sanz, B.M., Morcrette, J.J., Park, B.K., Peubey, C., de Rosnay, P., Tavolato, C., Thepaut, J.N., Vitart, F., 2011. The ERA-Interim reanalysis: configuration and performance of the data assimilation system. *Q. J. R. Meteorol. Soc.* 137, 553–597.
- Dockery, D.W., Pope, C.A., 1994. Acute respiratory effects of particulate air pollution. *Annu. Rev. Public Health* 15, 107–132.
- Fan, J., Wang, Y., 2016. Atmospheric emissions of As, Sb, and Se from coal combustion in Shandong Province, 2005–2014. *Pol. J. Environ. Stud.* 25, 2339–2347.
- Fischer, E., Perry, K.D., Jaffe, D.A., 2011. Optical and chemical properties of aerosols transported to Mount Bachelor during spring 2010. *J. Geophys. Res.* 116, D18202.
- Fu, H., Chen, J., 2017. Formation, features and controlling strategies of severe haze-fog pollutions in China. *Sci. Total Environ.* 578, 121–138.
- Fu, Q.Y., Zhuang, G.S., Wang, J., Xu, C., Huang, K., Li, J., Hou, B., Lu, T., Streets, D.G., 2008. Mechanism of formation of the heaviest pollution episode ever recorded in the Yangtze River Delta, China. *Atmos. Environ.* 42, 2023–2036.
- Gong, D.-Y., Ho, C.-H., 2002. The Siberian High and climate change over middle to high latitude Asia. *Theor. Appl. Climatol.* 72, 1–9.
- Grantz, D.A., Garner, J.H., Johnson, D.W., 2003. Ecological effects of particulate matter. *Environ. Int.* 29, 213–239.
- Hall, D.K., Riggs, G.A., 2015. MODIS/Terra Snow Cover Monthly L3 Global 0.05Deg CMG, Version 6. [Indicate subset used]. NASA National Snow and Ice Data Center Distributed Active Archive Center, Boulder, Colorado USA.
- Han, Z., Li, S.L., Mu, M., 2011. The role of warm North Atlantic SST in the formation of positive height anomalies over the Ural Mountains during January 2008. *Adv. Atmos. Sci.* 28, 246–256.
- Han, S.-Q., Wu, J.-H., Zhang, Y.-F., Cai, Z.-Y., Feng, Y.-C., Yao, Q., Li, X.-J., Liu, Y.-W., Zhang, M., 2014. Characteristics and formation mechanism of a winter haze-fog episode in Tianjin, China. *Atmos. Environ.* 98, 323–330.
- Harrison, R.M., Yin, J., 2000. Particulate matter in the atmosphere: which particle properties are important for its effects on health? *Sci. Total Environ.* 249, 85–101.
- He, S., Wang, H., 2016. Linkage between the East Asian January temperature extremes and the preceding Arctic Oscillation. *Int. J. Climatol.* 36, 1026–1032.
- He, S., Wang, H., Liu, J., 2012. Changes in the relationship between ENSO and Asia-Pacific midlatitude winter atmospheric circulation. *J. Clim.* 26, 3377–3393.
- Hong, Y.-C., Lee, J.-T., Kim, H., Ha, E.-H., Schwartz, J., Christiani, D.C., 2002. Effects of air pollutants on acute stroke mortality. *Environ. Health Perspect.* 110, 187–191.
- Hung, C.H., Lo, K.C., Yuan, C.S., 2018. Forming highly polluted PMs caused by the invasion of transboundary air pollutants: model simulation and discussion. *Aerosol Air Qual. Res.* 18, 1698–1719.
- Hur, S.-K., Oh, H.-R., Ho, C.-H., Kim, J., Song, C.-K., Chang, L.-S., Lee, J.-B., 2016. Evaluating the predictability of PM<sub>10</sub> grades in Seoul, Korea using a neural network model based on synoptic patterns. *Environ. Pollut.* 218, 1324–1333.
- Hwang, I., Hopke, P.K., 2007. Estimation of source apportionment and potential source locations of PM<sub>2.5</sub> at a west coastal IMPROVE site. *Atmos. Environ.* 41, 506–518.
- Hyslop, N.P., 2009. Impaired visibility: the air pollution people see. *Atmos. Environ.* 43, 182–195.
- Jang, E., Do, W., Park, G., Kim, M., Yoo, E., 2017. Spatial and temporal variation of urban air pollutants and their concentrations in relation to meteorological conditions at four sites in Busan, South Korea. *Atmos. Pollut. Res.* 8, 89–100.
- Jeong, J.-H., Ou, T., Linderholm, H.W., Kim, B.-M., Kim, S.-J., Kug, J.-S., Chen, D., 2011. Recent recovery of the Siberian High intensity. *J. Geophys. Res.* 116, D23102.
- Jeong, U., Kim, J., Lee, H., Lee, Y.G., 2017. Assessing the effect of long-range pollutant transportation on air quality in Seoul using the conditional potential source contribution function method. *Atmos. Environ.* 150, 33–44.
- Kim, K.-H., Kim, M.-Y., 2003. The effects of Asian Dust on particulate matter fractionation in Seoul, Korea during spring 2001. *Chemosphere* 51, 707–721.
- Kim, K.-H., Shon, Z.-H., 2011a. Long-term changes in PM<sub>10</sub> levels in urban air in relation with air quality control efforts. *Atmos. Environ.* 45, 3309–3317.
- Kim, K.-H., Shon, Z.-H., 2011b. Nationwide shift in CO concentration levels in urban areas of Korea after 2000. *J. Hazard. Mater.* 188, 235–246.
- Kim, K.-H., Sul, K.-H., Szulejko, J.E., Chambers, S.D., Feng, X., Lee, M.-H., 2015. Progress in the reduction of carbon monoxide levels in major urban areas in Korea. *Environ. Pollut.* 207, 420–428.
- Kim, H.-S., Chung, Y.-S., Yoon, M.-B., 2016. An analysis on the impact of large-scale transports of dust pollution on air quality in East Asia as observed in central Korea in 2014. *Air Qual. Atmos. Health* 9, 83–93.
- Kim, B.-U., Bae, C., Kim, H.C., Kim, E., Kim, S., 2017a. Spatially and chemically resolved source apportionment analysis: case study of high particulate matter event. *Atmos. Environ.* 162, 55–70.
- Kim, H.C., Kim, S., Kim, B.-U., Jin, C.-S., Hong, S., Park, R., Son, S.-W., Bae, C., Bae, M., Song, C.-K., Stein, A., 2017b. Recent increase of surface particulate matter concentrations in the Seoul Metropolitan Area, Korea. *Sci. Rep.* 7, 4710.
- Kim, H., Kim, H., Lee, J.-T., 2019. Effect of air pollutant emission reduction policies on hospital visits for asthma in Seoul, Korea; Quasi-experimental study. *Environ. Int.* 132, 104954.
- Koo, Y.-S., Yun, H.-Y., Choi, D.-R., Han, J.-S., Lee, J.-B., Lim, Y.-J., 2018. An analysis of chemical and meteorological characteristics of haze events in the Seoul metropolitan area during January 12–18, 2013. *Atmos. Environ.* 178, 87–100.
- Korea Ministry of Environment, 2015. The 4th National Environmental Comprehensive Plan for 2016–2035. Korea Ministry of Environment.
- Korea Ministry of Environment, 2017. Annual Report of Air Quality in Korea 2016. National Institute of Environmental Research.
- Lee, J., Kim, K.-Y., 2018. Analysis of source regions and meteorological factors for the variability of spring PM<sub>10</sub> concentrations in Seoul, Korea. *Atmos. Environ.* 175, 199–209.
- Lee, B.-K., Lee, H.K., Jun, N.-Y., 2006. Analysis of regional and temporal characteristics of PM<sub>10</sub> during an Asian dust episode in Korea. *Chemosphere* 63, 1106–1115.
- Lee, S., Ho, C.-H., Choi, Y.-S., 2011. High-PM<sub>10</sub> concentration episodes in Seoul, Korea: background sources and related meteorological conditions. *Atmos. Environ.* 45, 7240–7247.
- Lee, S., Ho, C.-H., Lee, Y.G., Choi, H.-J., Song, C.-K., 2013. Influence of transboundary air pollutants from China on the high-PM<sub>10</sub> episode in Seoul, Korea for the period October 16–20, 2008. *Atmos. Environ.* 77, 430–439.
- Lee, Y.G., Ho, C.-H., Kim, J.-H., Kim, J., 2015. Quiescence of Asian dust events in South Korea and Japan during 2012 spring: Dust outbreaks and transports. *Atmos. Environ.* 114, 92–101.
- Lee, H.-J., Kim, J.E., Cha, J.W., Song, S., Ryoo, S.-B., Kim, Y.P., 2018a. Characteristics of long-lasting haze episodes observed in Seoul, South Korea, for 2009–2014. *Theor. Appl. Climatol.* 136, 55–64.
- Lee, G., Oh, H.-R., Ho, C.-H., Park, D.-S.R., Kim, J., Chang, L.-S., Lee, J.-B., Choi, J., Sung, M., 2018b. Slow decreasing tendency of fine particles compared to coarse particles associated with recent hot summers in Seoul, Korea. *Aerosol Air Qual. Res.* 18, 2185–2194.
- Li, S., 2004. Impact of northwest Atlantic SST anomalies on the circulation over the Ural Mountains during early winter. *J. Meteorol. Soc. Jpn.* 82, 971–988.
- Li, T., Wang, H., Zhao, T., Xue, M., Wang, Y., Che, H., Jiang, C., 2016. The impacts of different PBL schemes on the simulation of PM<sub>2.5</sub> during severe haze episodes in the Jing-Jin-Ji region and its surroundings in China. *Adv. Meteorol.* 2016, 1–15.
- Liu, X., Hui, Y., Yin, Z.-Y., Wang, Z., Xie, X., Fang, J., 2016. Deteriorating haze situation and the severe haze episode during December 18–25 of 2013 in Xi'an, China, the worst event on record. *Theor. Appl. Climatol.* 125, 321–335.
- Luo, D., Xiao, Y., Yao, Y., Dai, A., Simmonds, I., Franzke, C.L.E., 2016. Impact of Ural blocking on winter warm Arctic-cold Eurasian anomalies. Part I: Blocking-induced amplification. *J. Clim.* 29, 3925–3947.
- North, G.R., Bell, T.L., Cahalan, R.F., 1982. Sampling errors in the estimation of empirical orthogonal functions. *Mon. Weather Rev.* 110, 699–706.
- Oh, H.-R., Ho, C.-H., Kim, J., Chen, D., Lee, S., Choi, Y.-S., Chang, L.-S., Song, C.-K., 2015. Long-range transport of air pollutants originating in China: a possible major cause of multi-day high-PM<sub>10</sub> episodes during cold season in Seoul, Korea. *Atmos. Environ.* 109, 23–30.
- Oh, H.-R., Ho, C.-H., Park, D.-S.R., Kim, J., Song, C.-K., Hur, S.-K., 2018. Possible relationship of weakened Aleutian Low with air quality improvement in Seoul, South Korea. *J. Appl. Meteorol. Climatol.* 57, 2363–2373.
- Park, S.S., Lee, K.-H., 2015. Characterization and sources of black carbon in PM<sub>2.5</sub> at a site close to a roadway in Gwangju, Korea, during winter. *Environ. Sci. Process. Impacts* 17, 1794–1805.
- Polissar, A.V., Hopke, P.K., Harris, J.M., 2001. Source regions for atmospheric aerosol measured at Barrow, Alaska. *Environ. Sci. Technol.* 35, 4214–4226.
- Rolph, G., Stein, A., Stunder, B., 2017. Real-time environmental applications and display system: READY. *Environ. Model. Softw.* 95, 210–228.
- Sanap, S.D., Pandithurai, G., 2015. Inter-annual variability of aerosols and its relationship with regional climate over Indian subcontinent. *Int. J. Climatol.* 35, 1041–1053.
- Seo, J., Kim, J.Y., Youn, D., Lee, J.Y., Kim, H., Lim, Y.B., Kim, Y., Jin, H.C., 2017. On the multiday haze in the Asian continental outflow: the important role of synoptic conditions combined with regional and local sources. *Atmos. Chem. Phys.* 17, 9311–9332.
- Shi, P., Zhang, G., Kong, F., Chen, D., Azorin-Molina, C., Guijarro, J.A., 2019. Variability of winter haze over the Beijing-Tianjin-Hebei region tied to wind speed in the lower troposphere and particulate sources. *Atmos. Res.* 215, 1–11.
- Shu, L., Xie, M., Gao, D., Wang, T.J., Fang, D.X., Liu, Q., Huang, A.N., Peng, L.W., 2017. Regional severe particle pollution and its association with synoptic weather patterns in the Yangtze River Delta region, China. *Atmos. Chem. Phys.* 17, 12871–12891.
- Stein, A.F., Draxler, R.R., Rolph, G.D., Stunder, B.J., Cohen, M.D., Ngan, F., 2015. NOAA's HYSPLIT atmospheric transport and dispersion modeling system. *Bull. Am. Meteorol. Soc.* 96, 2059–2077.
- Sun, S.D., Jiang, W., Gao, W.D., 2016. Vehicle emission trends and spatial distribution in Shandong province, China, from 2000 to 2014. *Atmos. Environ.* 147, 190–199.
- Tibaldi, S., Molteni, F., 1990. On the operational predictability of blocking. *Tellus* 42A, 343–365.
- Wai, K.-M., Tanner, P.A., 2005. Relationship between ionic composition in PM<sub>10</sub> and the synoptic-scale and mesoscale weather conditions in a south China coastal city: a 4-year study. *J. Geophys. Res.* 110, D18210.
- Wang, L., Chen, W., Zhou, W., Huang, R., 2009. Interannual variations of East Asian trough axis at 500 hPa and its association with the East Asian winter monsoon pathway. *J. Clim.* 22, 600–614.
- Wang, H., Tan, S.C., Wang, Y., Jiang, C., Shi, G.Y., Zhang, M.X., Che, H.Z., 2014. A multisource observation study of the severe prolonged regional haze episode over eastern China in January 2013. *Atmos. Environ.* 89, 807–815.
- World Health Organization, 2006. WHO Air Quality Guidelines for Particulate Matter, Ozone, Nitrogen Dioxide and Sulfur Dioxide. World Health Organization Regional Office for Europe, Copenhagen.
- Wu, B., Wang, J., 2002. Winter Arctic oscillation, Siberian High and East Asian winter monsoon. *Geophys. Res. Lett.* 29, 1897.
- Wu, B., Zhang, R., D'Arrigo, R., 2006. Distinct modes of the East Asian winter monsoon. *Mon. Weather Rev.* 134, 2165–2179.
- Xia, X.A., Chen, H.B., Wang, P.C., Zhang, W.X., Goloub, P., Chatenet, B., Eck, T.F., Holben, B.N., 2006. Variation of column-integrated aerosol properties in a Chinese urban region. *J. Geophys. Res.* 111, D05204.
- Xiao, Q., Ma, Z., Li, S., Liu, Y., 2015. The impact of winter heating on air pollution in

- China. PLoS One 10, e0117311.
- Xu, L., Batterman, S., Chen, F., Li, J., Zhong, X., Feng, Y., Rao, Q., Chen, F., 2017. Spatiotemporal characteristics of PM<sub>2.5</sub> and PM<sub>10</sub> at urban and corresponding background sites in 23 cities in China. *Sci. Total Environ.* 599–600, 2074–2084.
- Xu, G., Jiao, L.M., Zhao, S.L., Yuan, M., Li, X.M., Han, Y.Y., Zhang, B., Dong, T., 2016a. Examining the impacts of land use on air quality from a spatio-temporal perspective in Wuhan, China. *Atmosphere* 7.
- Xu, R., Tang, G., Wang, Y., Tie, X., 2016b. Analysis of a long-term measurement of air pollutants (2007–2011) in North China Plain (NCP); Impact of emission reduction during the Beijing Olympic Games. *Chemosphere* 159, 647–658.
- Yan, R.C., Yu, S.C., Zhang, Q.Y., Li, P.F., Wang, S., Chen, B.X., Liu, W.P., 2015. A heavy haze episode in Beijing in February of 2014: characteristics, origins and implications. *Atmos. Pollut. Res.* 6, 867–876.
- Yang, Y.R., Liu, X.G., Qu, Y., Wang, J.L., An, J.L., Zhang, Y., Zhang, F., 2015. Formation mechanism of continuous extreme haze episodes in the megacity Beijing, China, in January 2013. *Atmos. Res.* 155, 192–203.
- Yang, X., Jiang, L., Zhao, W., Xiong, Q., Zhao, W., Yan, X., 2018. Comparison of ground-based PM<sub>2.5</sub> and PM<sub>10</sub> concentrations in China, India, and the US. *Int. J. Environ. Res. Public Health* 15, 1382.
- Yao, Y., Luo, D.H., Dai, A.G., Simmonds, I., 2017. Increased quasi stationarity and persistence of winter Ural blocking and Eurasian extreme cold events in response to Arctic warming. Part I: insights from observational analyses. *J. Clim.* 30, 3549–3568.
- You, T., Wu, R., Huang, G., Fan, G., 2017. Regional meteorological patterns for heavy pollution events in Beijing. *J. Meteor. Res.* 31, 597–611.
- You, T., Wu, R., Huang, G., 2018. Differences in meteorological conditions between days with persistent and non-persistent pollution in Beijing, China. *J. Meteor. Res.* 32, 81–98.
- Zeng, Y., Hopke, P.K., 1989. A study of the sources of acid precipitation in Ontario, Canada. *Atmos. Environ.* 23, 1499–1509.
- Zhai, T., Zhao, Q., Gao, W., Shi, R., Xiang, W., Huang, H.-I.A., Zhang, C., 2015. Analysis of spatio-temporal variability of aerosol optical depth with empirical orthogonal functions in the Changjiang River Delta, China. *Front. Earth Sci.* 9, 1–12.
- Zhang, X.Y., Gong, S.L., Shen, Z.X., Mei, F.M., Xi, X.X., Liu, L.C., Zhou, Z.J., Wang, D., Wang, Y.Q., Cheng, Y., 2003. Characterization of soil dust aerosol in China and its transport and distribution during 2001 ACE-Asia: 1. Network observations. *J. Geophys. Res. Atmos.* 108, 4261.
- Zhang, H.F., Wang, S.X., Hao, J.M., Wang, X.M., Wang, S.L., Chai, F.H., Li, M., 2016. Air pollution and control action in Beijing. *J. Clean. Prod.* 112, 1519–1527.
- Zhang, H., Sun, X., Wang, W., 2017. Study on the spatial and temporal differentiation and influencing factors of carbon emissions in Shandong province. *Nat. Hazards* 87, 973–988.
- Zhang, Y.Q., Liu, C.G., Li, K., Zhou, Y., 2018a. Strategy on China's regional coal consumption control: a case study of Shandong province. *Energy Policy* 112, 316–327.
- Zhang, G., Xu, H.H., Qi, B., Du, R.G., Gui, K., Wang, H.L., Jiang, W.T., Liang, L.L., Xu, W.Y., 2018b. Characterization of atmospheric trace gases and particulate matter in Hangzhou, China. *Atmos. Chem. Phys.* 18, 1705–1728.
- Zhao, S.Y., Feng, T., Tie, X.X., Long, X., Li, G.H., Cao, J.J., Zhou, W.J., An, Z.S., 2018. Impact of climate change on Siberian High and wintertime air pollution in China in past two decades. *Earth's Future* 6, 118–133.
- Zheng, S., Cao, C.X., Singh, R.P., 2014. Comparison of ground based indices (API and AQI) with satellite based aerosol products. *Sci. Total Environ.* 488–489, 398–412.
- Zheng, B., Tong, D., Li, M., Liu, F., Hong, C.P., Geng, G.N., Li, H.Y., Li, X., Peng, L.Q., Qi, J., Yan, L., Zhang, Y.X., Zhao, H.Y., Zheng, Y.X., He, K.B., Zhang, Q., 2018. Trends in China's anthropogenic emissions since 2010 as the consequence of clean air actions. *Atmos. Chem. Phys.* 18, 14095–14111.
- Zhou, W., Chan, J.C.L., Chen, W., Ling, J., Pinto, J.G., Shao, Y.P., 2009. Synoptic-scale controls of persistent low temperature and icy weather over Southern China in January 2008. *Mon. Weather Rev.* 137, 3978–3991.
- Zhou, Y., Li, L., Hu, L., 2017. Correlation analysis of PM<sub>10</sub> and the incidence of lung cancer in Nanchang, China. *Int. J. Environ. Res. Public Health* 14, 1253.